Satellite-based evidence of dust emission over Northern Canada

Ian Ashpole[1], Aldona Wiacek[1,2]

[1]Department of Environmental Science, Saint Mary's University, Halifax, Canada
[2]Department of Astronomy and Physics, Saint Mary's University, Halifax, Canada

5 *Correspondence to*: Ian Ashpole (ian.ashpole@smu.ca)

Abstract. High latitude dust (HLD) is receiving growing research interest as its relative impact in the Arctic has been elucidated. Precise knowledge of HLD emission locations is limited in both field studies and satellite observations, leading to a general lack of representation in global models. Using the Frequency of Occurrence (FoO) of above-average Dust Optical Depth (DOD > 0.5) from twenty years (2002-2022) of high-resolution MODIS observations derived for this study (0.1° x 0.1°), we present quantitative evidence that dust sources are widespread across the Canadian Arctic Archipelago. Additionally, we present qualitative supporting evidence from aerosol type 'dust' classifications in VIIRS and CALIPSO satellite data products, as well as some challenges of comparing MODIS AOD to two co-located AERONET sites.

The HLD hotspots identified in the "Canadian Arctic Dust Belt" correspond to surfaces with high potential for dust emission in the G-SDS-SBM dataset. There are more areas where hotspots are observed but emission potential is low than the opposite case; additionally, two considerable areas of dust emission are identified at lower latitudes in mainland Canada. When spatially averaged across the broad dust producing region (65°N – 85°N, 125°W – 70°W), annual mean time series of FoO of MODIS DOD > 0.5 between 2003 and 2022 suggest an increase in the frequency of dustiness in the latter half of this period, consistent with our understanding that HLD emissions are increasing in a warming climate. These results further motivate model development to include HLD sources and provide an observational basis for evaluating them.

1 Introduction

Mineral dust aerosols (herein "dust") play an important role in the Earth System, for example through modifying the atmospheric and surface radiative budgets (Kok et al., 2018), influencing cloud processes (Tobo et al., 2019), providing nutrients to terrestrial (Nogueira et al., 2021) and oceanic (Dansie et al., 2022) ecosystems, and reducing the albedo of snow and ice when deposited (Sarangi et al., 2020) on these surfaces. Dust can also pose a significant health risk when particles are inhaled, with increased risk found for populations living downwind of source regions (Yang et al., 2022).

Dust emission depends upon high wind speeds occurring over surfaces where dust-sized particles (< ~100 μm) are available for entrainment. Therefore, the most dominant global dust hotspots are the hot subtropical deserts (e.g. Prospero et al., 2002; Washington et al., 2003), where a lack of surface moisture and vegetation create favourable conditions for emission to occur. However, dust sources in colder, mid-latitude regions have been shown to have a higher potential for interactions with high ice clouds, despite being much smaller dust emission sources (Wiacek et al., 2010). More recently, high latitude

regions have received growing research interest too, even though preferential dust source areas in the Arctic have been identified two decades ago (Tegen, 2003 and references therein). Although current best estimates suggest that they contribute only around 3 – 5%, by mass, to the global dust cycle (Bullard et al., 2016; Groot Zwaaftink et al., 2016), there is evidence that high latitude dust sources have a disproportionately large contribution to radiative forcing in the Arctic in comparison to
35   dust from lower latitudes, due to being the dominant contributor to near-surface loadings and deposition there (Groot Zwaaftink et al., 2016; Kylling et al., 2018). High latitude dust originates largely in glacial processes, which efficiently produce and deliver fine sediment to barren proglacial floodplains that are the prime emission hotspots when winds (which may be accelerated by regional ice sheets and glaciers) are strong enough (Bullard et al 2016). It is likely that the high latitude emissive areas will grow as a result of Arctic climate change impacts such as glacial retreat, decreased snow cover duration, and
40   permafrost thaw (Bullard, 2013; Meinander et al., 2022), further justifying their continued study.

Meinander et al. (2022) provide a comprehensive overview of high latitude dust, and use numerical modelling, data from the Global Sand and Dust Storms Source Base Map (G-SDS-SBM; Vukovic, 2021; 2022), and case study analysis to make the case for a northern high latitude dust belt. Of the 64 high latitude dust sources documented in that study, only 4 are in Canada. However, presented source intensity (SI) data from the G-SDS-SBM dataset (Fig. 2 in Meinander et al., 2022) suggests that
45   large portions of the land surface in Northern Canada have high potential to emit dust under favourable wind conditions. The study's conclusion calls for an increase in observational studies aimed at identifying new high latitude dust sources, without which accurate modelling of known dust effects is not possible. That is the aim of this paper, with a focus on Northern Canada.

While products such as the G-SDS-SBM can highlight surfaces that have the potential to emit dust, observations of dust storms actually occurring are necessary to classify areas as sources. To this end, datasets derived from satellite instruments are
50   crucial to understanding the global distribution of dust, with areas where dust is most frequently detected determined to be source locations (e.g. Prospero et al., 2002; Washington et al., 2003; Ginoux et al., 2012). Dust detection by these remote sensing methods is based on the exceedance of a threshold value in retrieval products that quantify the amount of aerosol present in the atmospheric column, such as aerosol optical depth (AOD; e.g. Ginoux et al., 2012; Baddock et al., 2016), or binary presence/absence data based on retrieval criteria related to dust (e.g. Ashpole and Washington, 2012). Information on
55   the vertical location of dust in the atmospheric column, provided by instruments such as the Cloud-Aerosol Lidar with Orthogonal Polarization (CALIOP), can also be used to determine the presence of dust source regions, with low altitude dust likely to be proximal to a source (Todd and Cavazos-Guerra, 2016). Since satellite measurements are sensitive to the influence of all aerosol types, not just dust, results are typically verified using additional independent data sources, such as ground observations (when available), retrievals from other satellite instruments, or simulated dust fields from numerical models.
60   Unfortunately, ground observations are few and far between in many known or likely source regions owing to their remoteness, with the combination of environmental variables required for dust emission to occur in the first place being unfavourable for human habitation.

To date, satellite data have only been used to study individual source areas in northern Canada on a case study basis (Ranjbar et al., 2021; Huck et al., 2023). The key objective of this paper is to use satellite datasets to identify where dust is

65 detected most frequently across the whole of northern Canada. The primary dataset used is derived from the Moderate
Resolution Imaging Spectroradiometer (MODIS) AOD, which has been widely used to identify dust source areas on a global
(Ginoux et al., 2012) and regional (Baddock et al., 2016) basis, but not at high latitudes. Covering a 20+ year period, data from
MODIS also enable an assessment of temporal changes in dustiness. "Aerosol Type" data from the Visible Infrared Imaging
Radiometer Suite (VIIRS) instrument, and information on the vertical location of "dust" aerosol type in the atmospheric

70 column from CALIOP are used as comparison datasets to evaluate results from MODIS. Findings are compared to SI from G-
SDS-SBM to assess whether the satellite-derived dust hotspots correspond to surfaces with high emissive capacity; and, finally,
our satellite datasets are verified against surface AOD observations from two Aerosol Robotic Network (AERONET) stations
in northern Canada.

2 Data and methods

75 ### 2.1 Satellite-derived aerosol datasets

2.1.1 MODIS

This study uses Dust Optical Depth (DOD), derived from Aerosol Optical Depth (AOD) data, to map the distribution of dust
aerosols. DOD is a widely used quantity that estimates what portion of retrieved AOD is due to extinction by mineral dust
particles alone, as opposed to the total contribution to AOD from all aerosols. First employed to map the distribution of dust

80 sources on a global scale by Ginoux et al. (2012), DOD calculations use retrievals of Ångström exponent (α) and single
scattering albedo (ω) to isolate the dust contribution to AOD; α is a measure of how AOD changes with wavelength and is
highly sensitive to particle size (Eck et al., 1999). Dust aerosols are typically coarser (particle radius > 1 µm) than urban and
biomass burning aerosols (particle radius < 1 µm, Dubovik et al., 2002), although the dust size distribution tends towards
smaller radii as distance from source areas increases due to the gravitational settling of larger particles. For coarse mode

85 particles, values of α are low or even negative. The fraction of light that is scattered compared to the total extinction optical
depth, which is a function of both scattering and absorption, is given by ω. Dust absorbs solar radiation and is therefore
characterised by ω values < 1, separating it from purely scattering coarse aerosols such as a sea salt.

There are various DOD formulations in the literature, and this study employs two of them:

90 1. DOD is calculated according to the method of Pu and Ginoux (2016; herein denoted as DOD_{PG16}), whereby DOD is
calculated from every AOD retrieval based on an empirically derived continuous function relating α to AOD
(Anderson et al., 2005):

$$DOD_{PG16} = AOD \times (0.98 - 0.5089\alpha + 0.0512\alpha^2), \text{ if } \omega < 1; \tag{1}$$

95

2. DOD is simply the AOD value for those retrievals where α is less than a threshold value. Different studies have used different α thresholds, and here the value of 0.3 is applied following Baddock et al. (2016, herein denoted DOD_{B16}), which employed DOD to precisely analyse dust sources in the Chihuahuan Desert, one of the most active dust regions in North America. For clarity:

100

$$DOD_{B16} = AOD, \text{ if } \alpha < 0.3 \text{ and } \omega < 1. \tag{2}$$

Both DOD formulations are derived to highlight the coarse-mode fraction of dust only, optimising them for dust source identification since the coarse-mode is estimated to account for more than 90% of particles at emission (Kok et al., 2017), and

105 since coarse mode particles remain closer to source regions.

The DOD datasets used in this study are derived from MODIS aerosol products retrieved using the "Deep Blue" algorithm. Deep Blue employs radiance measurements in the blue channels to detect aerosols globally over land, even over bright surfaces such as deserts. The algorithm exploits the fact that because surface reflectance is low and less variable at blue channels, increases of reflectance and spectral contrast indicate the presence of aerosols (Hsu et al., 2013). Our study uses Deep Blue

110 aerosol products from the MODIS instrument (Sayer et al., 2015) carried onboard the Aqua satellite, which passes the equator at around 13:30 local time (ascending node). Products (AOD, α, ω, and various quality flags – see below) are taken from the MODIS Level 2 Joint Atmosphere product ("ATML2"), collection 6.1 (Platnick et al., 2017), with aerosol parameters stored at 10 km spatial resolution in 5-minute time interval swath files. For the Aqua satellite, these files are denoted "MYDATML2". Data were downloaded from the NASA Level-1 and Atmosphere Archive and Distribution System Distributed Active Archive

115 Centre (https://ladsweb.modaps.eosdis.nasa.gov/search/order/2/MYDATML2--61, last access 11 January 2024). For computational efficiency, only files that contained data in the region spanning (150º W – 50º W, 40º N – 85º N) were obtained, for the time period spanning 2002-07-04 to 2022-12-31 (the whole period covered by the MYDATML2 dataset at the time this study was undertaken). The products used in this study were regridded from their Level 2 swath files to a regular 0.1º x 0.1º grid using nearest neighbour interpolation and mosaiced daily, thereby creating a high-resolution Level 3 product optimised

120 for this study.

It is recommended that only aerosol products flagged as "very good" (QA = 3) are used for scientific analysis (Hsu et al., 2013). However, Baddock et al., (2016) clearly demonstrate the detrimental effect that this has for dust source detection, because of highly variable AOD values over 10 x 10 pixels of 1 km each, upon which the data quality flags are based, proximal to dust sources. Filtering for QA = 3 resulted in a fivefold loss of data and far fewer source detections in their work. This study

125 therefore follows the recommendation of Baddock et al., (2016) to include data of all quality levels (QA = 1 – 3) in the analysis. However, a sensitivity analysis is performed comparing results to those obtained by applying the QA = 3 filter (Sect. 3.1).

2.1.2 VIIRS

Information on aerosol type is obtained from Visible Infrared Imaging Radiometer Suite (VIIRS) Deep Blue aerosol products, which include an "aerosol type" classification. The classification is based on Deep Blue AOD and Ängstrom Exponent (α)

130   retrievals, as well as a series of smoke tests, based on the spectral variation of measured reflectance. The algorithm is outlined in detail and verified against other satellite products/imagery and AERONET data by Hsu et al., (2019). In brief, retrievals are given the aerosol type classification "dust" when:

- AOD > 0.3,
- Smoke tests determine the retrieval not to be smoke,

135   - α < 0.5.

The AOD > 0.3 threshold is applied to minimise the effect of variable surface reflectance in the visible wavelengths; retrievals not meeting this threshold are given the "background" aerosol type. Where the AOD threshold is met, smoke is ruled out, and α > 1, the aerosol type is set to "non-smoke fine mode", while those retrievals with an Ängstrom exponent between 0.5 and 1 are determined to be "mixed type" aerosols. It should be noted that retrievals performed over clouds or snow/ice

140   surfaces are excluded from the product, as are retrievals performed over coastal pixels, to avoid subpixel mixed surface-type issues (since the surface type determines whether aerosol retrievals are performed using the Deep Blue algorithm (land) or Satellite Ocean Aerosol Retrieval (SOAR) algorithm).

VIIRS aerosol products used in this study are from the VIIRS sensor carried onboard the Suomi National Polar-orbiting Partnership (S-NPP) satellite, which has an equator crossing time (ascending) of 13:30 local time. Level 2

145   "AERDB_L2_VIIRS_SNPP" files were downloaded from the NASA Level-1 and Atmosphere Archive and Distribution System Distributed Active Archive Centre (doi.org/10.5067/VIIRS/AERDB_L2_VIIRS_SNPP.002, https://ladsweb.modaps.eosdis.nasa.gov/search/order/1/AERDB_L2_VIIRS_SNPP--5200, last access 11 January 2024).Version 2.0 data are used. As with MODIS data, only files that contained data in the region spanning (150º W – 50º W, 40º N – 85º N) were obtained, for the period spanning 2020-01-01 to 2022-12-31 (a three-year subset of the period covered by

150   MODIS data used in this study). Likewise, data were regridded from their Level 2 swath files (native resolution 6 x 6 km^2) to a regular 0.1º x 0.1º grid using nearest neighbour interpolation and mosaiced daily.

2.1.3 CALIOP

To obtain information on the vertical distribution of dust in the atmosphere – specifically to address the question of whether it is close to the surface and therefore indicative of local emission – aerosol type classification data from the Cloud-Aerosol

155   Lidar with Orthogonal Polarization (CALIOP) are used. CALIOP products have been used in global aerosol source attribution studies (Prijith et al., 2013), and the vertical information in retrievals has been exploited to detect dust emission at the surface in the Sahara Desert (Todd and Cavazos-Guerra, 2016). CALIOP is carried onboard the Cloud-Aerosol Lidar and Infrared Pathfinder Satellite Observations (CALIPSO) platform, which also has an equator crossing time of 13:30 local time

160 (ascending). CALIOP has been making vertical profile measurements of the Earth's atmosphere on a global scale since June 2006 and provides information on layer types for both clouds and aerosols (Winker et al., 2010). Its aerosol classification algorithm uses altitude, location, surface type, estimated particulate depolarization ratio, and integrated attenuated backscatter to identify the aerosol subtype (Kim et al., 2018; Omar et al., 2009); aerosol type "dust" corresponds to total attenuated backscatter > 0.075 and estimated depolarization ratio > 0.20.

For this study, the CALIPSO lidar Level 3 (L3) tropospheric aerosol profile "all sky" product, Version 4.20 is used
165 ("CAL_LID_L3_Tropospheric_APro_AllSky-Standard-V4-20" files). Parameters included in the L3 files are derived from the Version 4 CALIOP Level 2 aerosol profile product; prior to aggregating, L2 data are quality screened to reduce the impact of e.g. layer detection or classification errors. Level 2 data are aggregated monthly on a grid of dimensions 5° longitude x 2.5° latitude x 60 metres vertical (for altitudes between -0.5 and 12 km) (Tackett et al., 2018). This level of aggregation compensates for the ~70 m footprint of the laser on the ground, produced every 333 m, during each orbit (compared to MODIS
170 and VIIRS orbital swaths of 2330 km and 3060 km, respectively). This study uses the "aerosol type" parameter from the L3 files. The "aerosol type" parameter stores the monthly sums of the number of Level 2 samples ("sample" equals the number of measurement opportunities within the grid cell) having the CALIPSO aerosol types "clean marine", "dust", "polluted continental/smoke", "clean continental", "polluted dust", "elevated smoke", and "dusty marine" within each L3 latitude/longitude/altitude grid cell. Results presented here are based only on analysis of the "dust_nsamples" parameter, i.e.,
175 "polluted dust" and "dusty marine" are excluded. Data were downloaded from the NASA Earthdata portal (https://search.earthdata.nasa.gov/search, last access 11 January 2024), for the period spanning June 2006 – July 2020 inclusive. Only daytime files were used in the analysis.

2.2 Other datasets

Data from the Global Sand and Dust Storms Source Base Map ("G-SDS-SBM"; Vukovic, 2021; 2022) were used as an
180 independent source of information to verify the dust emission potential of the satellite-identified dust hotspot areas. Specifically, the source intensity parameter was used, "SI", with values from 0 (no capacity to emit dust) to 1 (maximum capacity in cases of strong surface winds). G-SDS-SBM was developed by the United Nations Convention to Combat Desertification (UNCCD) in collaboration with the United Nations Environment Programme (UNEP) and World Meteorological Organization (WMO). It is derived using information on soil texture, bare land fraction, land cover, topsoil
185 moisture, topography, and temperature. Values of SI represent the maximum potential of the surface to emit dust under favourable wind conditions between the years 2014-2018, and are available for the months of January, April, July, and October. SI data were regridded from their native 30 arcsec resolution (~0.008°) to 0.1° to match the MODIS data used in this study.

For verification of satellite-based results, data from the Aerosol Robotic Network (AERONET; Holben et al., 1998) are used. AERONET is a network of ground-based sun photometers that retrieve AOD and other atmospheric properties in the
190 column above the instrument, based on solar extinction within the column. This study uses data from two stations in the broad study region of northern Canada: Kluane Lake (Yukon; 61.027°N, 138.410°W) and Resolute Bay (Nunavut; 74.705°N,

94.969°W; station locations are marked on Fig. 11). The Kluane Lake AERONET station was intentionally located proximal to a known dust source with the purpose of monitoring emission processes there (e.g. Huck et al., 2023), and has been providing data between April and November since 2018 (with varying temporal coverage by year). Resolute Bay is an Arctic monitoring

195   site, providing data since 2004 (also with varying temporal coverage, also restricted to the months of April – November). Arctic aerosol studies have demonstrated that the site detects transported Asian dust during the spring and smoke aerosols during the summer, and that during summer months the area is also subject to wind-induced sea-salt-spray aerosol and potentially dust derived from more localised sources, based on the analysis of retrieved particle size distributions (Tomasi et al., 2015; AboEl-Fetouh et al., 2020).

200   Data from both stations were downloaded from the AERONET website (https://aeronet.gsfc.nasa.gov/, last access 11 January 2024), and this study analyses Level 1.5 AOD retrievals at 500 nm, processed by the Version 3 algorithm (Giles et al., 2019). Only retrievals performed within 11 am and 5 pm local time were considered for analysis (which roughly corresponds to a 6-hour window centred on the local overpass time of both satellites). The maximum retrieved AOD each day within this time window was retained for comparison to satellite-derived parameters.

205   Two additional datasets are used in this study. Firstly, wind fields discussed in Sect. 3.6 are taken from the European Centre for Medium-Range Weather Forecasts Reanalysis Version 5 (ERA-5), with a spatial resolution of 0.28125 degrees (~ 31 x 31 km) and 137 vertical levels (Hersbach et al., 2020; downloaded from the Copernicus Climate Data Store at https://doi.org/10.24381/cds.143582cf, last access 11 January 2024). Surface elevation data, also discussed in Sect. 3.6, are taken from the Global Multi-resolution Terrain Elevation Data 2010 dataset (GMTED2010; Danielson and Gesch, 2011,

210   downloaded from https://www.temis.nl/data/gmted2010/index.php, last access 11 January 2024), at 0.0625° resolution.

3 Results and discussion

3.1 Inferences about dust over Canada from MODIS

Since DOD values will be elevated by both locally sourced and long-range transported dust, this study applies a threshold to DOD data to identify areas of persistently high dust loadings, which we assume to be largely undiluted and locally sourced

215   dust. A high frequency of occurrence (FoO) of DOD above a specified threshold relative to the surrounding region is commonly used to indicate a local dust source region (e.g. Ginoux et al., 2012; Baddock et al., 2016). The FoO is simply the total number of observations in the time series that meet a given DOD threshold, expressed as either an absolute value or a relative value given the total number of observations in the time series. DOD threshold selection is somewhat subjective and depends upon the amount of long-range transported dust present in the atmosphere as well as the intensity of local emission. For example,

220   Ginoux et al., (2012) apply a DOD threshold of 0.2 globally and experiment with higher and lower thresholds regionally; Baddock et al., (2016) applies a DOD threshold of 0.75 to pinpoint sources on a landscape-scale; and Pu et al., (2020) experiment with DOD thresholds ranging from 0.02 for less dusty regions to 0.5 for global dust hotspots such as North Africa. This study considers results using DOD thresholds of 0.5 and 1.

Maps of FoO DOD$_{PG16}$ > 0.5 show several distinct features (Fig. 1a). There is a broad swath of FoO > ~50 in southern
225 Alberta and Saskatchewan, extending across the border with the United States; this feature is associated with croplands, as
discussed more fully in Section 3.2. The remaining northern features are of more interest to the high latitude dust question:
most notably, numerous spatially discrete dust hotspots (FoO > 80) scattered across the islands (north of 70°N) that make up
Canada's Arctic Archipelago. There are a few additional isolated FoO hotspots in continental northern Canada, for example
in southern Northwest Territories close to the border with the Yukon Territory (MacKenzie Mountains, pink square in Fig.
230 11), scattered across northern continental Nunavut, and at the border between northern Québec and Labrador (blue square in
Fig. 11). Many of these hotspots correlate with 'barren land' classifications in the Canadian Land Cover Atlas. Notably, the
greatest FoO values are in the Arctic Archipelago, as opposed to further south where dust is perhaps more commonly expected
to be present.

The pattern in FoO DOD$_{B16}$ > 0.5 is very similar to that in FoO DOD$_{PG16}$ (Fig. 1b), with two exceptions. Firstly, FoO
235 values are around 50% lower in the DOD$_{B16}$ dataset; secondly, the northern FoO hotspots tend to be focussed east of 95°W in
DOD$_{B16}$, whereas they are distributed more evenly across the full longitudinal extent of Canada's north in DOD$_{PG16}$. Lower
FoO values may be expected in DOD$_{B16}$ than DOD$_{PG16}$, because the former is only calculated for subsets of AOD retrievals
that meet certain filtering criteria (α < 0.3), whereas the latter is calculated for all AOD retrievals with no filtering applied (see
DOD equation outlined in Sect. 2.1.1.)

240 MODIS AOD retrievals – upon which DOD is based – are more numerous at southern latitudes than in the far north (Fig.
1 g-i) for reasons such as cloud and snow cover, and the lack of reflected visible radiation during northern winter (polar night
of varying duration occurs north of 67°N) which is required to make AOD retrievals. To account for this, FoO DOD > 0.5
values are normalised across the study domain by dividing the FoO count by the number of available DOD retrievals. The
resulting maps for both DOD datasets (Fig. 1d-e) show that the relative frequency of DOD > 0.5 is far greater in the north than
245 for the broad DOD hotspot across the Canada-US border, with values exceeding 50% in DOD$_{PG16}$ and reaching 100% in
DOD$_{B16}$ (values closer to 100% are more likely in DOD$_{B16}$ than DOD$_{PG16}$ due to its threshold-based derivation, as mentioned
above).

The same threshold of 0.5 is applied to the parent AOD data (Fig 1c, f). Overall FoO AOD > 0.5 values are greater across
Canada, as expected, but the northern hotspots remain with FoO exceeding 200 at some locations. The greater values for FoO
250 AOD > 0.5 across Canada, in regions where FoO DOD is close to zero, shows the value of using DOD data to highlight the
contribution of dust particles to the retrieved AOD value, against the contribution from other aerosols which are present in the
atmosphere.
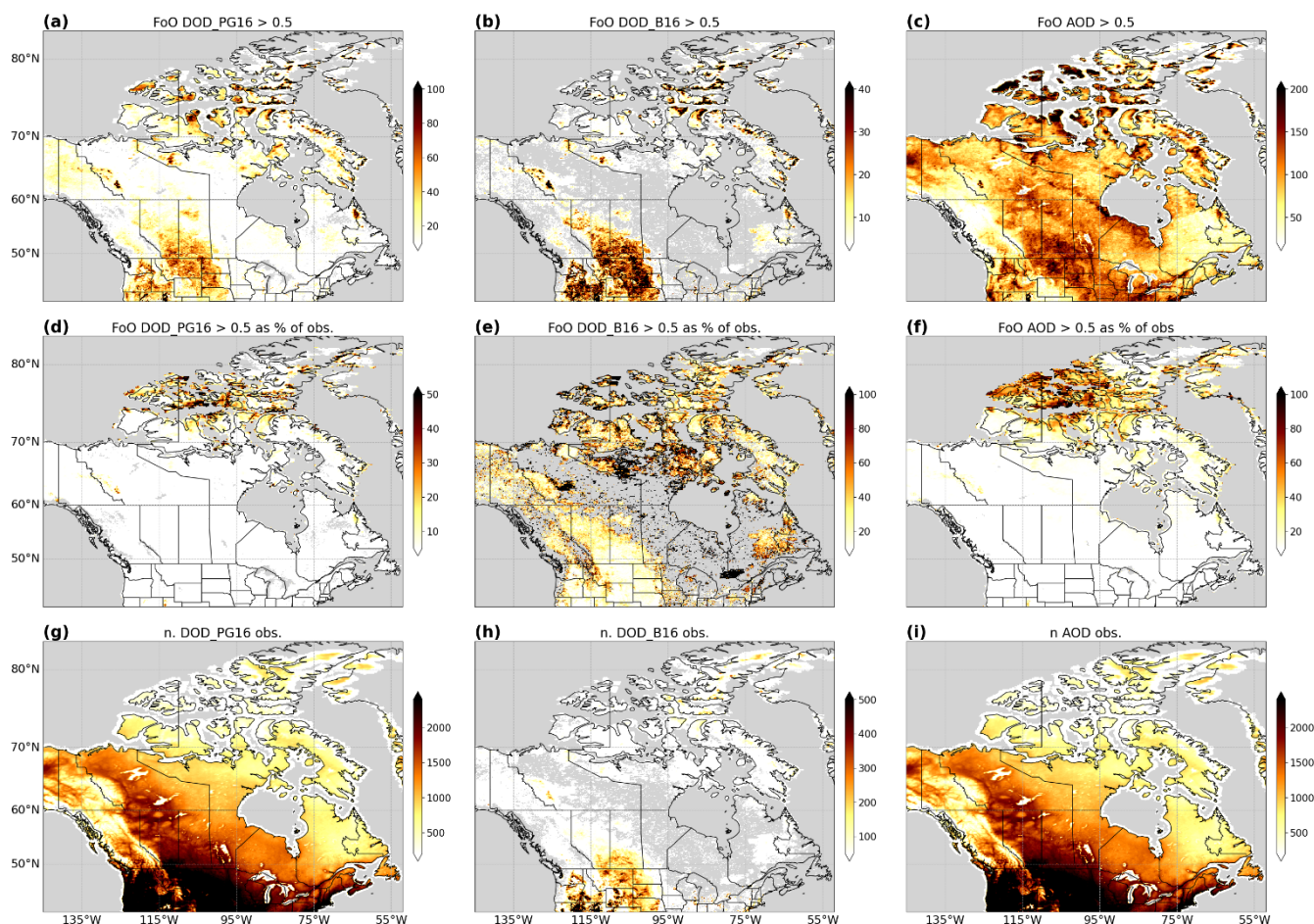
Figure 1. Frequency of Occurrence (FoO) of **a)** $DOD_{PG16} > 0.5$, **b)** FoO $DOD_{B16} > 0.5$, and **c)** FoO AOD > 0.5. FoO as a percentage of the number of retrievals available for **d)** $DOD_{PG16} > 0.5$, **e)** $DOD_{B16} > 0.5$, and **f)** AOD > 0.5. Number of retrievals available for **g)** DOD_{PG16}, **h)** DOD_{B16}, and **i)** AOD. Note the different colour scales used. Grey shading corresponds to no data. All panels are based on MODIS data for 2003 – 2022.

If the DOD (or AOD) threshold is increased to 1, FoO values decrease (maximum values < 20) and the spatial extent of hotspots contracts (compare Fig. 2a and Fig. 2b for a comparison of FoO DOD_{PG16} with the thresholds of 0.5 and 1 respectively; note that maps for FoO $DOD_{B16} > 1$ and FoO AOD > 1 are included in Supp. Mat. 1). However, many spatially discrete hotspots in the north remain in attenuated form (compare Fig. 2d, e).

There are no DOD products north of 70°N between the months of October and April inclusive (Fig. 3, left column). This is to be expected due to a combination of a) polar night during parts of the winter preventing satellite AOD retrievals based on visible wavelengths and b) the fact that much of the surface is frozen, which inhibits the atmospheric entrainment of surface-

derived dust particles. For these reasons, DOD retrievals in the north predominantly occur during the months of June, July, and August (Fig. 3, right column), with May and September representing the shoulder seasons (Fig. 3, middle column).
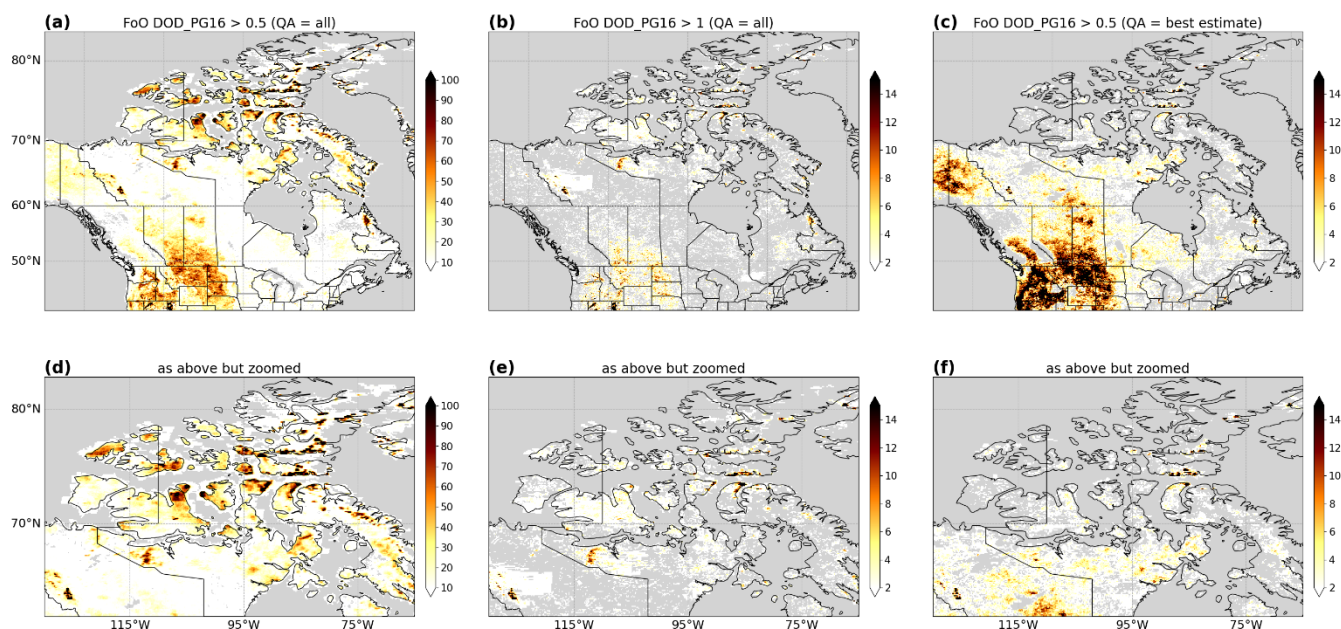
Figure 2. a) Frequency of Occurrence **(**FoO) of $DOD_{PG16} > 0.5$, using data at all quality levels (i.e. not screened for "best estimate" quality flag). Note that this is a reproduction of Fig. 1a. **b)** FoO $DOD_{PG16} > 1$, using data at all quality levels. **c)** FoO $DOD_{PG16} > 0.5$, using data screened for "best estimate" quality flag. **d-f)** as a)-c) but zoomed to better highlight northern DOD hotspots. Grey shading corresponds to no data. All panels are from MODIS data for 2003 – 2022.

The results discussed in Figs. 1 and 2 thus far are based on AOD retrievals that are not filtered using the data quality flag that is distributed with the data. As discussed at the end of Sect. 2.1.1, this is based on the findings of Baddock et al., (2016), wherein the DOD based on the unfiltered AOD dataset was of greater value for dust source detection – a core aim of this paper – as opposed to DOD calculated using only the AOD retrievals that remain after filtering for the "best estimate" quality flag. The present analysis was replicated after applying the "best estimate" quality flag filter to the AOD data to test the effect of this choice. This resulted in a big reduction in FoO DOD (and AOD) > 0.5 values and a consequent contraction of the hotspot areas (Figs. 2c and 2a show a comparison of FoO $DOD_{PG16} > 0.5$ with and without the "best estimate" quality flag filter, respectively; note that equivalent maps for DOD_{B16} and AOD are included in Supp. Mat. 2), however many of the isolated hotspots in the north remain in attenuated form (compare Figs. 2d and 2f). The spatial patterns in these maps are similar to those of FoO $DOD_{PG16} > 1$ created using data unfiltered by the quality flag (Figs. 2b and 2e).

The dust hotspots inferred in this section from MODIS DOD data will be evaluated against the dust emission potential map in Sect. 3.4, examined over time in Sect. 3.5, and evaluated against AERONET stations in Sect. 3.6.
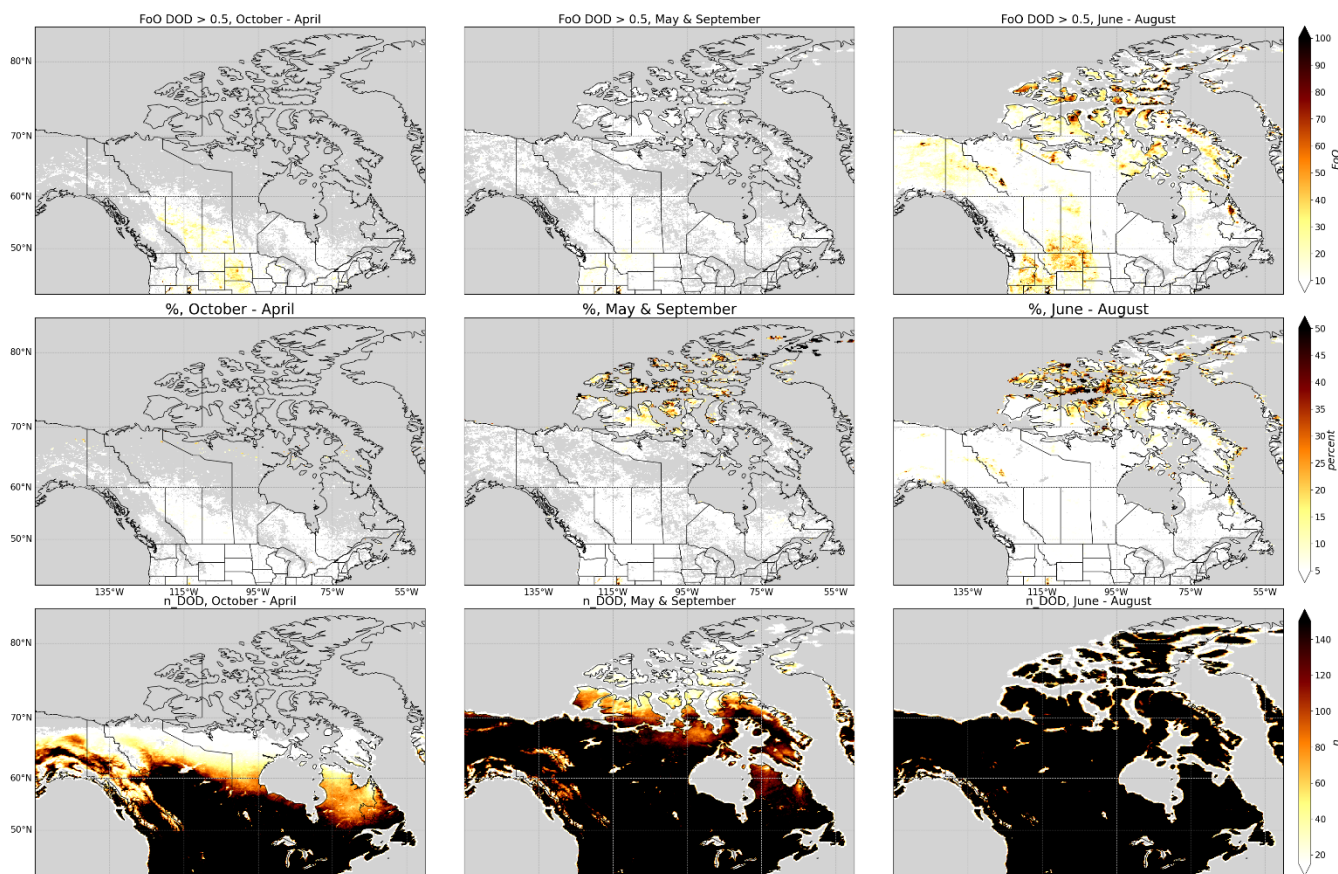
Figure 3. Seasonal cycle in DOD_{PG16} over Canada (MODIS data spans 2003 – 2022). **Top row)** FoO DOD_{PG16} > 0.5, by season. **Middle row)** FoO DOD_{PG16} > 0.5 as a percentage of the number of DOD_{PG16} retrievals, by season. **Bottom row)** number of DOD_{PG16} retrievals, by season. **Left column)** October – April inclusive (winter season). **Middle column)** May and September (shoulder season). **Right column)** June – August inclusive (summer season). Grey shading corresponds to no data.

3.2 Inferences about dust over Canada from VIIRS

The frequency with which VIIRS aerosol retrievals were classified as aerosol type "dust" (FoO AT_{DUST}) for the period 2020 – 2022 is shown in Fig. 4a. Greatest FoO AT_{DUST} values are seen north of 65°N over land, with values exceeding 80 in some hotspot regions for the 3-year period. When represented as a percentage of the number of all aerosol type retrievals, dust is clearly the dominant retrieval type over much of the land area of northern Canada (Fig. 4d), accounting for > 80% of all aerosol type retrievals in some hotspots. However, it should be noted that some of these high percentage areas have quite low FoO AT_{DUST} (< 10), and a low number of aerosol type retrievals overall, too. We note that AT_{DUST} is also being retrieved over water (Fig. 4a) with increasing frequency towards lower latitudes and a stark land-water contrast (both over open salt water

300 and inland fresh water like the Great Lakes). This FoO feature is attenuated in the relative representation of FoO in Fig. 4c, even though the land-water contrast remains; we do not interpret it as dust.
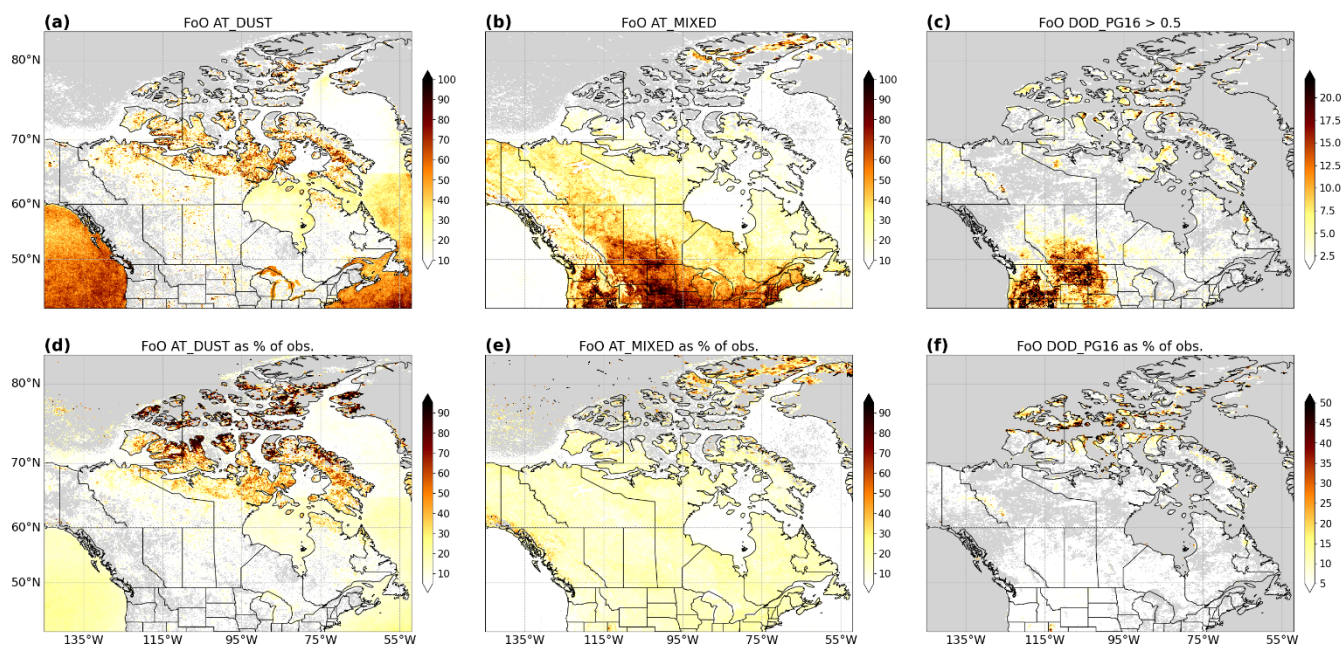
Figure 4. Frequency of Occurrence (FoO) of **a)** VIIRS aerosol type (AT) = "dust" (AT_{DUST}), **b)** VIIRS AT = "mixed"
305 (AT_{MIXED}), and **c)** MODIS $DOD_{PG16} > 0.5$. FoO expressed as a percentage of the number of available retrievals for **d)** AT_{DUST},
e) AT_{MIXED}, and **f)** MODIS $DOD_{PG16} > 0.5$. Note the different colour scales used. Grey shading corresponds to no data. All
panels are from data only for the period 2020 – 2022 inclusive.

Aside from dust, there are large areas with an aerosol type classification of "mixed" (FoO AT_{MIXED}) north of ~80° N on
310 Ellesmere Island and in the surrounding region (Fig. 4b), accounting for a high proportion (> 60 %) of total aerosol type
retrievals there (Fig. 4e). Mixed aerosol type is also widespread south of 70°N, reaching peak values in south-central Canada
and extending across the border with the US, where it accounts for 20 – 30% of all aerosol type retrievals (with most of the
other retrievals being classified either as "smoke", "non-smoke fine mode", or "background" aerosol type – see Supp. Mat. 3
for an analysis of additional aerosol types not considered in this study). Mixed aerosol type ($0.5 < \alpha < 1$) is indicative of
315 smaller particles than the large dust aerosol type ($\alpha < 0.5$), but smaller clay fraction (< 2 μm) dust particles in fact dominate
the emitted *number* size distribution (e.g., Kok et al., 2011), and they are found both close to sources and also after long-range
transport (e.g., Prospero et al., 1999; Zhao et al., 2022); therefore, we interpret VIIRS mixed aerosols as likely dust indicators,
where they occur as discrete source areas (as opposed to a homogeneous background) and where they coincide with areas of
high emission potential in the dust emission potential map (Sect. 3.4).

320   For direct comparison, FoO DOD$_{PG16}$ > 0.5 is shown for the sub-period 2020 – 2022 (Fig. 4c, f). It is apparent that in the
north, peak FoO AT$_{DUST}$ is greater than peak FoO DOD$_{PG16}$ > 0.5 and that the area of FoO AT$_{DUST}$ is larger than it is for FoO
DOD$_{PG16}$ > 0.5. However, such differences are to be expected since these datasets are derived differently (as outlined in Sect.
2.1). Specifically, the FoO AT$_{DUST}$ map will include dust that did not pass the DOD$_{PG16}$ > 0.5 threshold (i.e., VIIRS AT$_{DUST}$
requires AOD > 0.3 with α < 0.5, while MODIS DOD$_{PG16}$ > 0.5 requires, e.g., AOD > 0.74 if α = 0.5 and AOD > 0.51 if α =
325   0; Eq. 1). Nonetheless, there is agreement between the two datasets on numerous hotspot areas across northern Canada. Lastly,
the large southern hotspot evident in FoO DOD$_{PG16}$ > 0.5 (Fig 4c) is likely fine dust emitted and transported in the large area
sources of the Great Plains of Canada and the US; this is consistent with the spatial coincidence with a peak in FoO AT$_{MIXED}$
in the Great Plains (Fig. 4b), where croplands are found, and where finer dust is expected to be mixed with anthropogenic
aerosols. The dust hotspots inferred in this section from VIIRS 'dust' aerosol type data will be evaluated against the dust
330   emission potential map in Sect. 3.4.

3.3 Inferences about dust over Canada from CALIOP

To analyse the vertical distribution of atmospheric dust over northern Canada, "aerosol type" classification data from CALIOP
were used. As outlined in Sect. 2.1.3, this product shows the number of times an aerosol of type "dust" (dust aerosol types
"polluted dust" and "dusty marine" were excluded as they are not the focus of this study) is detected in a bin of 5° longitude x
335   2° latitude x 60 m vertically, per month. The monthly totals were summed for JJA 2006 – 2020, inclusive, and these period-
sum values were then averaged for the latitude band 60°N – 80°N. A longitude-height plot of the resulting data (Fig. 5) shows
clear evidence of enhanced dust detection frequency at low altitudes for the longitude range between 125° W – 75° W, in good
agreement with the longitudinal range spanned by the dust hotspot regions identified in both the MODIS and VIIRS datasets
previously discussed. That dust detection frequency values are lower at higher altitudes across this region, and immediately to
340   the east and west of the region, suggests that the low-altitude enhancement in dust detection is due to increases in dustiness
within the region, implying surface sources of emission there. Also evident from this analysis are near-surface enhancements
in dust detection frequency between ~50°W and 25°W, as well as between 25°W and 15°W; these indicate emission from
sources in Greenland and Iceland, respectively, which have been documented elsewhere (see, e.g., Meinander et al., 2022).
The dust location information from CALIOP informs our analysis but is not suitable for direct comparison against the dust
345   emission potential map (Sect. 3.4) on account of the coarse spatial aggregation necessary to compensate for the 70-m laser
footprint (Sect. 2.1.3).
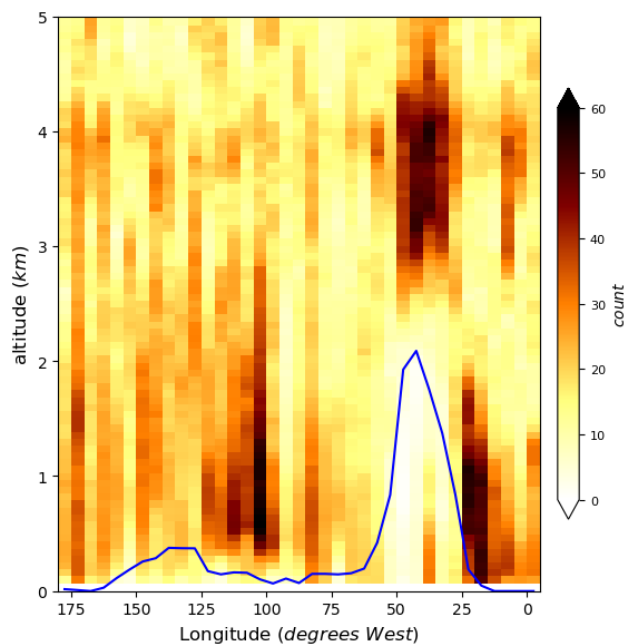
Figure 5. Number of times ('count') an aerosol is classified as "dust" in CALIOP L3 aerosol type data for the period JJA 2006 – 2020, averaged for the latitude band 60 – 80º N. The blue line shows the corresponding median surface elevation within the latitude band.

3.4 Evaluation of satellite dust hotspot results using the dust emission potential map

We turn now to comparing our satellite results with known information on dust emission potentials, the latter under favourable wind conditions. In Fig. 6 we compare MODIS FoO DOD_{PG16} > 0.5 and VIIRS FoO AT=Dust to source intensity (SI) for July from the G-SDS-SBM dataset. SI for July was chosen based on the results of the seasonal analysis in Sect. 3.1, where all-season FoO was dominated by June-July-August FoO in absolute terms and in spatial extent, and the fact that SI values are low for other months provided in the G-SDS-SBM dataset (SI for other months is plotted in Supp. Mat. 4). The dust emission potential is high (SI > 0.5) in much of Canada's Arctic Archipelago (Fig. 6a), which is broadly consistent with MODIS FoO DOD_{PG16} > 0.5 (Fig. 1a) and VIIRS FoO AT=Dust (Fig. 4a). We quantified areas of SI overlap with both MODIS (Fig. 6b, red colour) and VIIRS (Fig. 6c, red colour) using threshold SI and FoO values as follows. Because SI is a relative measure of dust emission potential with values between 0 (no emission potential under any wind conditions) and 1 (maximum emission potential under sufficient wind conditions), we looked for areas where SI is greater than 0.5 while, simultaneously, MODIS FoO is greater than 10%. This MODIS threshold was chosen because we are testing for the FoO of strong dust emission events (DOD > 0.5), and it is reasonable to assume that such conditions will be met in less than 0.5 (50%) of observational cases. Red colours indicate agreement between dust emission potential (SI) and satellite observations, while blue and green colours both indicate disagreement. Blue disagreement areas have high dust emission potential that is not matched with observations

of dust, while green disagreement areas have low dust emission potential where satellites nevertheless see high DOD (> 0.5) in at least 10% of observations. For consistency we report here the same 10% threshold in VIIRS FoO AT=Dust data, which leads to relatively prominent green areas (low emission potential but frequent VIIRS-observed dust) because, unlike MODIS FoO data, VIIRS FoO data considers only the presence of dust (VIIRS AT=Dust) and not the intensity of events (i.e., MODIS

370   DOD > 0.5). While the thresholds can be manipulated to an extent, influencing the level of agreement and disagreement and thus the spatial colour patterns, the key point is that all three datasets have limitations, yet all three point to non-zero dust activity north of 60°N, in contrast to many model simulations of dust emission to date that have ignored these high latitude dust sources, albeit reasonably so, e.g., on account of low model resolution or lack of input information. The key dust emission areas shared by all three datasets (shared orange and red colours) are found in a broad "Canadian Arctic Dust Belt" between

375   the horn-like Brodeur Peninsula of westernmost Baffin Island (~71°N, ~85°W) and northwest of Prince Patrick Island (~79°N, ~125°W). The same area also contains few blue colours (high emission potential but few observations of dust) but many green colours, where emission potential is low (< 0.5) but satellite observations show strong (MODIS) and/or frequent (VIIRS) dust events. The latter indicates areas where dust emission potential maps require re-examination and/or verification, i.e., also with new field measurements, challenging as they are.

380
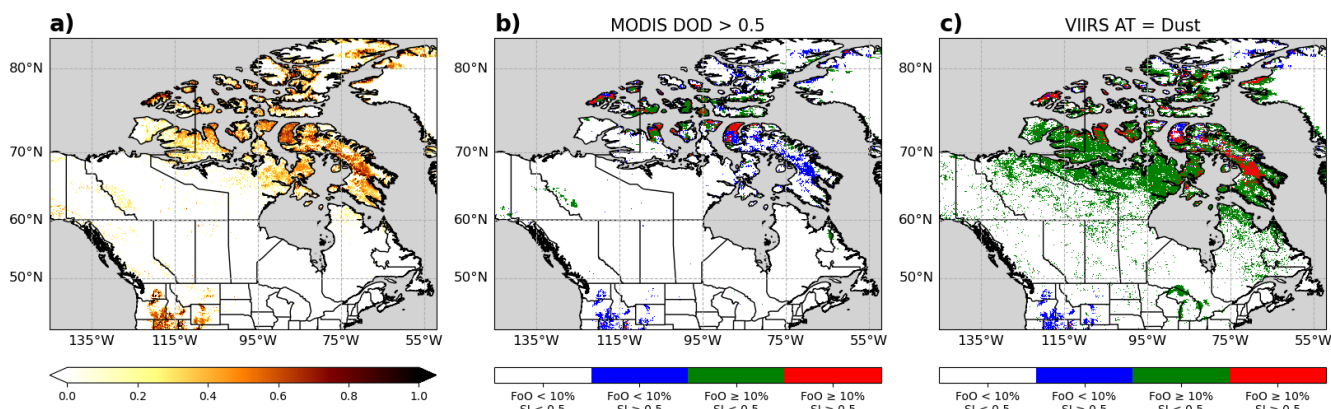
Figure 6. a) Source intensity (SI) from the G-SDS-SBM dataset for July. **b)** Combined classification map based on SI and FoO MODIS DOD$_{PG16}$ > 0.5 as a percentage of the number of DOD$_{PG16}$ retrievals available; **c)** Combined classification map based on SI and FoO VIIRS AT$_{DUST}$ as a percentage of the number of VIIRS Aerosol Type (AT) retrievals available. Grey

385   shading indicates no data.

The notable inconsistencies in the Arctic Archipelago include eastern Baffin Island (~70°N, ~75°W), which is characterised by widespread high SI (except in areas permanently covered by snow and ice) but sparse MODIS FoO DOD$_{PG16}$ > 0.5 hotspots (blue colours in Fig. 6b) with more frequent low-intensity VIIRS FoO AT=Dust regions (red colours in Fig.

390   6c). The same is true for ice-free parts of Ellesmere Island and Axel Heiberg Island (~80°N, ~85°W). One explanation for such

discrepancies, apart from thresholding choices, is that high SI values only show surfaces where the *potential* for dust emission is high; other conditions still need to be met for dust emission to actually occur, i.e. surface winds that are strong enough to entrain sediment. Another factor is that we have filtered MODIS data for DOD > 0.5, which represents strong dust emission events, on par with Saharan dust in transport across the tropical Atlantic, whereas our VIIRS data shows all observations of

395   pure (unpolluted) dust. On the other hand, it is plausible that the satellite datasets also do not capture the full extent of dustiness across the region, especially in the far north, due to frequent cloud coverage and dust misclassification as clouds (e.g., Huck et al., 2023; Ranjbar et al., 2021).

There are also a few notable areas south of the Arctic where FoO $DOD_{PG16} > 0.5$ hotspots are not matched by high SI, e.g., green domains in Fig. 6b in the Northwest Territories (MacKenzie Mountains), close to the border with the Yukon

400   Territory (~126°W, ~63°N) and at the border of northern Labrador and Québec (65°W, 58°N), as marked in Fig. 11. Reasons for such disagreements are unclear, but we stress again that the G-SDS-SBM SI mapping results are sensitive to the quality of the input data (soil texture, soil moisture, soil temperature, and bare land fraction), which all have limitations. In examining the visible imagery (Appendix), average wind speeds and geological features of these two discrepancy areas available from the Global Wind Atlas (Davis et al., 2023), there is strong indication that both, although geologically distinct, are likely

405   unclassified dust hotspot source areas. The MacKenzie Mountains location (Fig. A1), between the Keele River and Nahanni National Park, shows intense weathering and erosion in the area of the Redstone Plateau, leading to some colluvial and landslide features, and abundant alluvial fans, terraces, and flood plains (Boydell and Rutter, 1980; Duk-Rodkin and Huntley, 2018). The latter are comprised of sand, silt and minor gravel and represent sediments from modern to post-glacial drainage. The Labrador / Québec location (Fig. A2), east-southeast of Ulittaniujalik National Park, is the exposed and weathered Torngat

410   plateau. The area was recently deglaciated (Occhietti et al., 2004), leaving behind regionally atypical glacial sand, silty sand, and gravel (Brouard et al., 2020), with scarce vegetation and a thin soil profile that promotes dust mobilization. Clearly, further investigation is needed, including with field measurements.

Lastly, the broad swath of only occasionally high FoO $DOD_{PG16} > 0.5$ in the Great Plains of southern Canada and USA (connected to croplands and discussed in Sect. 3.2, Figs. 4b and 4c) is also largely not matched by high SI; this is reasonable

415   because this extensive pattern of occasional dustiness disappears in a percentage-of-observations representation (Figs. 4e and 4f), i.e., the satellite data is showing infrequent events of dust transported from confined sources. SI hotspots in this region (unlike the FoO signature, found only in northwestern US and not southwestern Canada) are much more spatially restricted than the FoO signature and comprise a mixture of croplands (Washington, northern Oregon, Idaho) and arid regions (southern Oregon, eastern Montana, Wyoming), but they do not correspond to either intense MODIS $DOD_{PG16} > 0.5$ events (Fig. 6b,

420   blue colours) or VIIRS AT=Dust events (Fig. 6c, blue colours). Instead, they are associated with VIIRS AT=Mixed (Figs. 4b and 4e), which, again, makes sense given that agricultural dust emissions are mixed with anthropogenic aerosols and transported over a broad region.

Overall, the reasonable agreement between satellite-derived dust hotspots and areas with high SI values in the G-SDS-SBM dataset supports the use of the satellite datasets in dust emission modelling development in the Canadian Arctic and in other high-latitude regions. This section also suggested regions where the SI dataset may benefit from further development.

3.5 Temporal change in intense dustiness frequency over Northern Canada in the 20-year MODIS record

The 20-year record of MODIS data enables an assessment of whether the frequency of dustiness over Northern Canada has changed over time. Time series of annual means of FoO DOD_{PG16} > 0.5, FoO DOD_{B16} > 0.5, and FoO AOD > 0.5, averaged for the region (65°N – 85°N, 125°W – 70°W), are shown in Fig. 7. This averaging area subsumes the broad "Canadian Arctic Dust Belt" identified in Sect. 3.4. Note that this figure shows values of mean FoO rather than mean optical depth, and that left and right y axes with different scales are employed to better show the (always) larger mean FoO AOD > 0.5. There is clear interannual variability in each of the time series; however, the greatest annual mean FoO DOD_{PG16} > 0.5 values all occur in the second half of the period, with 2017, 2019, 2014, 2015 (in descending order of mean FoO) appearing to be peak dust emission years. The same is true with FoO DOD_{B16} > 0.5, although the pattern is much less pronounced, with no peak for 2014. By contrast, the annual mean FoO AOD > 0.5 time series is qualitatively different, with peaks and troughs relatively evenly distributed across the study period. This suggests that any increase in AOD across the 20-year period may be driven by coarser, dust-sized particles, which the DOD datasets emphasise. As noted in Sect. 1, an increase in high latitude dust emission is an expected consequence of climate change in the Arctic leading to glacial retreat, decreased snow cover duration, and permafrost thaw, all making exposed dust more available (Bullard, 2013; Meinander et al., 2022). Our result is consistent with such processes occurring in the Arctic (Gulev et al., 2021).
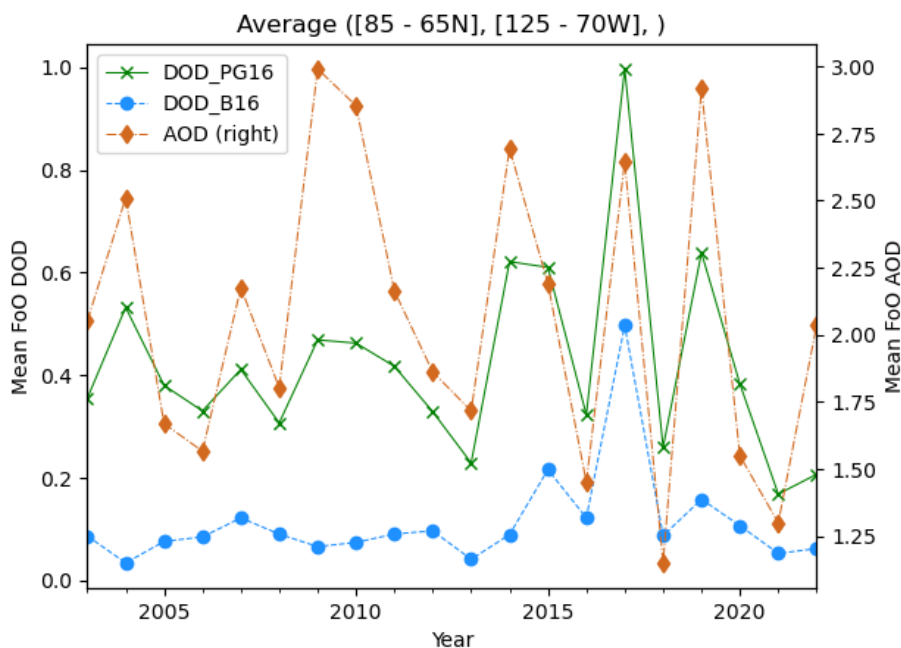
Figure 7. Time series of annual mean FoO of MODIS optical depth > 0.5, averaged for the region (65°N – 85°N, 125°W – 70°W), for the years 2003 – 2022 inclusive. MODIS optical depth datasets underlying the FoO values plotted are: DOD_{PG16} > 0.5, DOD_{B16} > 0.5, and AOD > 0.5.

3.6 Evaluation of MODIS AOD using AERONET

AOD data from MODIS are evaluated against AOD data from AERONET stations at Kluane Lake (AOD_{KL}) and Resolute Bay (AOD_{RB}). The station locations are marked on Fig. 11. The Kluane Lake AERONET station was intentionally located proximal to a known dust source with the purpose of monitoring emission processes there (Huck et al., 2023). Curiously, the area is not identified as a strong potential dust source area by our satellite data analysis, which is on the one hand not very surprising given that Huck et al. (2023) document large discrepancies between remotely sensed dust (both by AERONET and by MODIS-MAIAC) and *in situ* remote camera images of dust at Kluane Lake. On the other hand, their "dust event days" (DED's) have modal AOD values of 0.5 with a high tail extending out to an AOD of 3; in the context of such thick dust plumes, one may reasonably expect that in the analysis of 20 years of MODIS data in our study (Collection 6.1 at 10-km resolution) we would detect a stronger signal in FoO – yet we do not. However, the Kluane Lake region and the nearby mountainous regions, are largely without satellite data due to the extremely variable and highest topography in North America (Mt. Logan in Canada stands at 6,000 m and Denali in Alaska to the west stands at 6,200 m), which presents difficult surface retrieval conditions (as shown in detail later in Fig. 10). Unlike Kluane Lake, the Resolute Bay AERONET station is situated adjacent to strong potential dust emission hotspots identified in our study on Cornwallis Island (as shown in detail later in Fig. 10); however, to the best of our knowledge, this is coincidental, i.e., the station location was not selected with the explicit purpose of monitoring

dust aerosol. In this section, satellite data retrieved within both a 1° x 1° and 0.5° x 0.5° box centred on each AERONET station were considered. From MODIS, the maximum AOD values within the search box were retained, while from VIIRS the presence or absence of each aerosol classification type (AT) was recorded. For AERONET, only retrievals performed within 11 am and 5 pm local time were considered for analysis and the maximum retrieved AOD each day within this time window was retained for the comparison.

465

AOD comparison results are first considered using MODIS data detected within the 1° x 1° search box centred on the respective AERONET station. At Kluane Lake, six years of AOD_{KL} data correlates strongly with MODIS AOD (R = 0.87 in Fig. 8a). These AOD correlation results are at odds with the work of Huck et al. (2023) at Kluane Lake who find weak mean AOD (unlike our maximum AOD) correlations on "dust event days" in 2018 and 2019 (R = 0.11 and R= 0.36), which improve

470 on non-DED's in 2018 and 2019 (R = 0.35 and R = 0.96). They classify DED's with threshold AOD and α parameters similar to our work (but from their AERONET data) and they use the mean MODIS-MAIAC AOD product at 470 nm with the mean AERONET AOD product at 500 nm. Given their *in situ* remote camera imagery verifying the presence of dust, they reasonably attribute the lack of correlation on "dust event days" to specific dust-cloud detection problems in AERONET and the lack of dust testing at high latitudes in the MODIS-MAIAC dataset (rather than to the less important 470 nm vs. 500 nm wavelength

475 mismatch between MODIS and AERONET AOD). Their sampling strategy is different and covers just 70 km^2 with 1-km MODIS-MAIAC pixels as opposed to our 1° x 1° box based on 10-km resolution L2 MODIS data. While it is not possible to compare the results directly, it is nevertheless interesting to note both the range of choices and results in this apparently 'similar' type of comparison carried out in our respective studies. When three years of VIIRS AT data are present

480
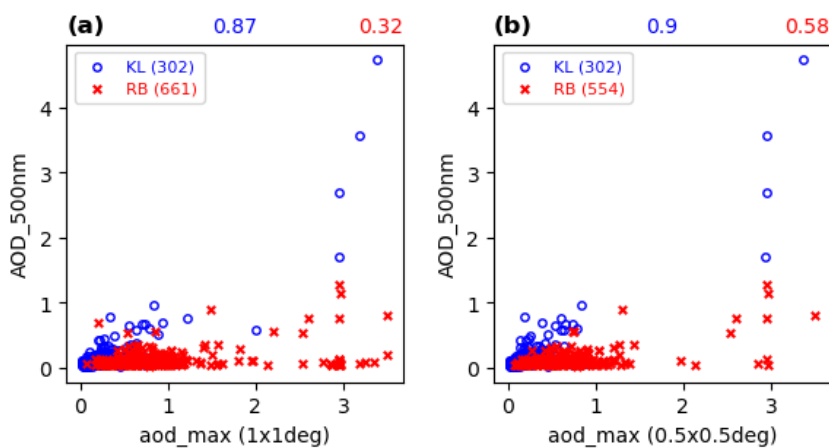
Figure 8. Maximum AERONET AOD (500 nm) between 11 am and 5 pm local time at Kluane Lake (blue open circles) and Resolute Bay (red crosses) vs. maximum MODIS AOD **a)** from a 1° x 1° box centred on each station; **b)** from a 0.5° x 0.5° box centred on each station. Numbers in blue (red) above each panel correspond to the Pearson's correlation coefficient, R,

between Kluane Lake (Resolute Bay) AERONET AOD and the MODIS dataset in that panel. The number of matched
maximum AOD days for each comparison is given in parentheses in the legends.
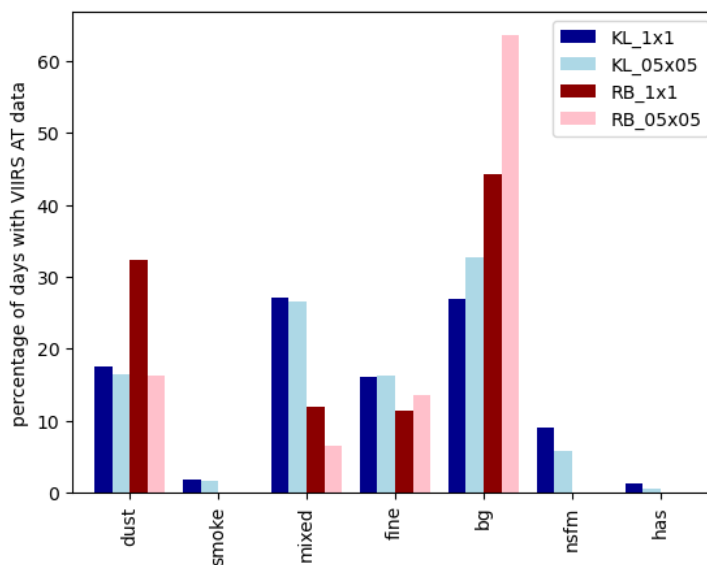
Figure 9. Percentage of days with VIIRS Aerosol Type (AT) data that have at least one AT retrieval of the type indicated on
the x-axis within the 1º x 1º and 0.5º x 0.5º boxes centred on AERONET stations at Kluane Lake (KL; dark and light blue,
respectively) and Resolute Bay (RB; dark and light red, respectively). "bg" = background, "nsfm" = non-smoke fine mode,
"has" = high-altitude smoke. The number of days with VIIRS AT data in the 1º x 1º (0.5º x 0.5º) box is 1278 (852) at
Kluane Lake and 429 (228) at Resolute Bay, both for the period 2020-2022.
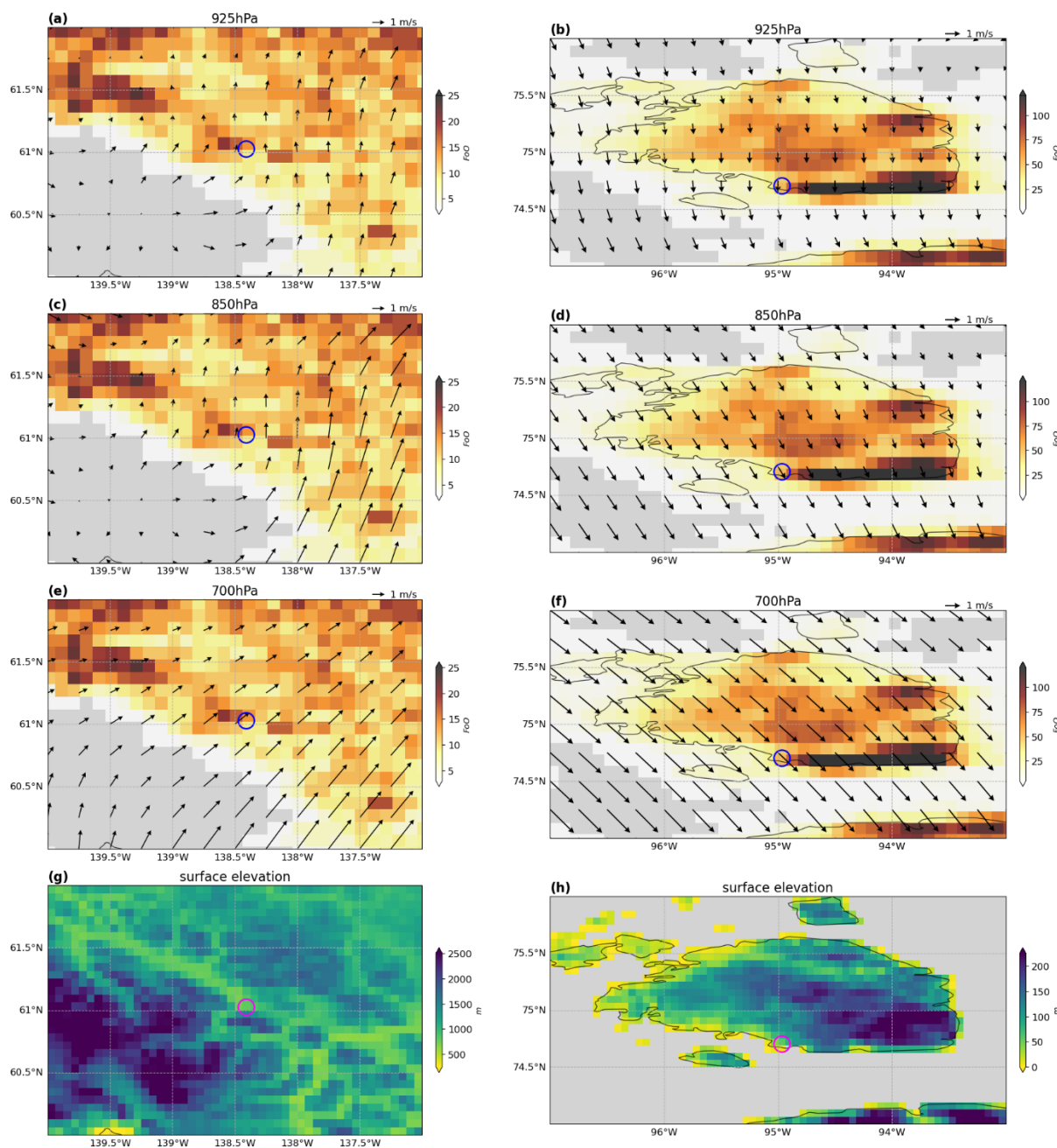
Figure 10. a,c,e) Winds at 925 hPa, 850 hPa, and 700 hPa above the region surrounding the Kluane Lake AERONET station (blue circle). Winds are the mean of ERA-5 reanalysis data for Jun. – Aug. 2004 – 2023. Underlying shading corresponds to FoO DOD$_{PG16}$ > 0.5 for the period 2003 – 2022 (grey shading corresponds to no data). **g)** Surface elevation surrounding Kluane Lake station (red circle) at 0.0625 degrees resolution from the Global Multi-resolution Terrain Elevation Data 2010 (GMTED2010) dataset. **b,d,f,h)** Like a,c,e,g) except for Resolute Bay AERONET station.

over the 1° x 1° region surrounding the Kluane Lake AERONET station, AT_{DUST} is detected on 18% of days while AT_{MIXED} and $AT_{BACKGROUND}$ are the two modal classifications, both detected on 27% of days (Fig. 9). Unlike at Kluane Lake, 18

500   years of Resolute Bay AOD_{RB} has only a weak correlation (R = 0.32) with MODIS AOD for the 1° x 1° search area (Fig. 8a). As Fig. 9 shows, VIIRS AT_{DUST} is detected on 32% of days here, with $AT_{BACKGROUND}$ being detected more frequently (44% of days) and AT_{MIXED} less frequently (12% of days).
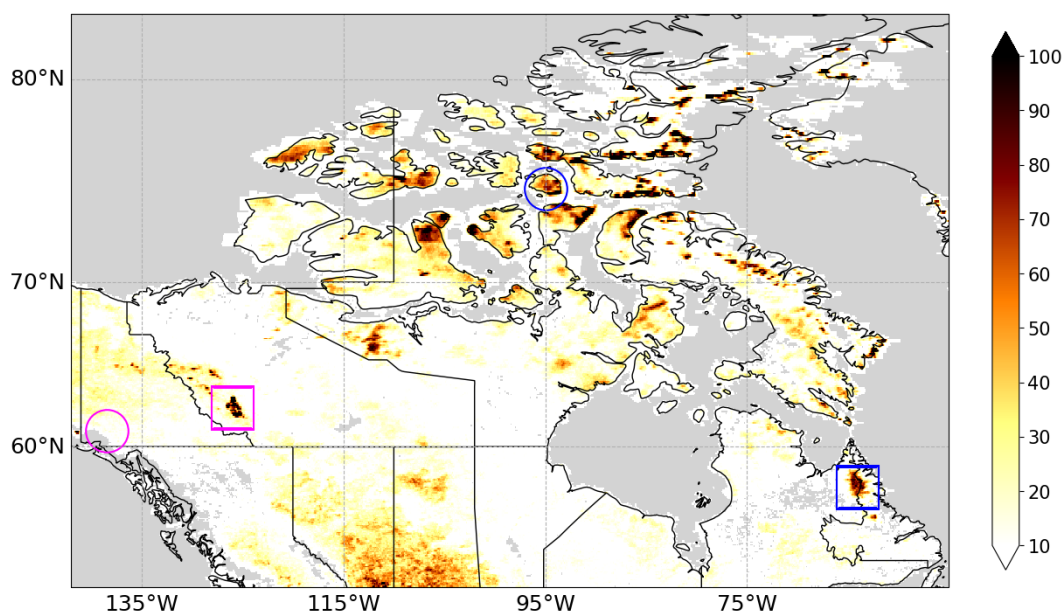
Figure 11. The location of Kluane Lake AERONET station (pink circle) and Resolute Bay AERONET station (blue circle),
together with new dust source areas in the McKenzie Mountains (pink square) and Quebec/Labrador (blue square).
Underlying shading corresponds to FoO DOD_{PG16} > 0.5 for the period 2003 – 2022 (grey shading corresponds to no data).

A question arises about the poor correlation at Resolute Bay between AERONET AOD_{RB} and MODIS AOD datasets

510   given the proximity to our potential hotspot regions and the more frequent VIIRS AT_{DUST} presence there. One reason could be the deliberate positioning of an AERONET station to monitor dust at a known emission location (like Kluane Lake), which was not the case for Resolute Bay (notwithstanding the AOD disagreement at Kluane Lake found by Huck et al, 2023 using the MODIS-MAIAC product). Is it possible that coarse dust in the 1° x 1° search area around Resolute Bay is simply not passing over the AERONET station, given that coarse dust does not generally travel far? The map of average regional winds

515   above both stations (Fig. 10) shows that Kluane Lake is downwind of dust emission regions in the foothills of the mountains (where satellite data is increasingly lacking on account of the variable topography and surface properties) while Resolute Bay is upwind of the dust emission hotspot (identified with abundant satellite data). The elevated topography to the east of Resolute Bay may itself obscure any dust suspended in that direction from the AERONET instrument's field of view for low solar zenith

angles in the morning. As may be expected in this situation, the correlation between MODIS AOD and AOD_{RB} increases from

520   0.32 to 0.58 as the MODIS search area is decreased from 1° x 1° to 0.5° x 0.5°, while the MODIS AOD correlation with AOD_{KL}

hardly changes (0.87 vs. 0.90) under the same decrease (Fig. 8b). Since the AERONET station at Kluane Lake is already next

to and downwind of the dust, decreasing the search area is not helpful to the correlation. Interestingly, this same decrease in

search area size causes the AT_{DUST} classification frequency at Resolute Bay to decrease from 32% for 1° x 1° to 16% for 0.5°

x 0.5°, while the $AT_{BACKGROUND}$ classification frequency increases from 44% to 64% (Fig. 9); there is no appreciable change

525   at Kluane Lake. This reduction supports the argument that dust in the broader region surrounding Resolute Bay is not within

detection range of the AERONET station and highlights the challenge of detecting even nearby dust sources given the station's

position and prevailing winds.

4 Summary and conclusions

High latitude mineral dust is receiving growing research interest, with evidence that its impacts on numerous components of

530   the Arctic environment are greater than for dust transported into the region from lower latitudes. Understanding these processes

– and how they change in the future – depends upon precise knowledge of where dust emission occurs at high latitudes, yet

field measurements are exceedingly difficult (and therefore scarce) and satellite-based retrievals of suspended dust suffer from

known high-latitude biases (polar night, increased cloudiness, bright surfaces). Using the Frequency of Occurrence (FoO) of

above-average Dust Optical Depth (DOD > 0.5) from twenty years (2002-2022) of high-resolution MODIS observations

535   derived for this study (0.1° x 0.1°), we present quantitative evidence that dust sources are widespread across the islands of the

Canadian Arctic Archipelago. Additionally, qualitative supporting evidence is presented from aerosol type 'dust' classification

in the VIIRS (α < 0.5 with AOD > 0.3) and CALIPSO (total attenuated backscatter > 0.075 with depolarization ratio > 0.20)

satellite data products.

The locations identified as dust hotspots (DOD > 0.5 with FoO > 10%) in the "Canadian Arctic Dust Belt"

540   (overwhelmingly based on retrievals from June to August) correspond to surfaces with high potential for dust emission during

the summer season in the G-SDS-SBM dataset (Source Intensity, SI > 0.5). However, there are significant areas of

disagreement in this region, where MODIS data shows dust (FoO > 10%) but the G-SDS-SBM dataset shows lower emission

potential (SI < 0.5); there are fewer areas where MODIS data does not show dust (FoO < 10%), but emission potential is higher

(SI > 0.5), notably on the southern portion of the Brodeur Peninsula of Baffin Island. Additionally, two considerable areas of

545   disagreement emerge at lower latitudes in mainland Canada (MacKenzie Mountains and the border between northern Québec

and Labrador), which we show to be potential dust emitting regions based on their geological features. The main limitation of

this comparison is the use of threshold FoO and SI values, which can be manipulated to an extent, influencing the level of

agreement and disagreement. However, the key point is that both datasets point to non-zero dust activity north of 60°N, in

contrast to many model simulations of dust emission to date that have ignored these high latitude dust sources, albeit reasonably

550   so, e.g., on account of low model resolution or lack of input information.

When spatially averaged across the larger dust producing region (65°N – 85°N, 125°W – 70°W), annual mean time series of FoO of MODIS DOD > 0.5 between 2003 and 2022 suggest an increase in the frequency of dustiness in the latter half of the period, which is consistent with our understanding that high latitude dust emissions are likely increasing in a warming climate.

555   The MODIS AOD product used in our study compares well (R = 0.87) to AOD from the AERONET station at Kluane Lake in Yukon Territory. While Kluane Lake is a known dust source area receiving focussed research attention, it is not a prominent dust emission hotspot in our study, likely because satellite retrievals are less frequent in the mountainous terrain. Nevertheless, the AERONET station was positioned downstream of known dust emission sources leading to good agreement with fewer data points. Conversely, the comparison is poor (R = 0.32) between our MODIS AOD product and AOD from the

560   AERONET station at Resolute Bay, Nunavut, with approximately double the data points. This AERONET station is situated close to satellite-derived dust hotspots in our study, however, its location is not well suited to detecting dust plumes emitted in the region because the emission hotspots are downstream of the station (on average). Somewhat unsurprisingly, station location is critical for verifying satellite-derived dust aerosols; this becomes even more important when the dust product specifically targets coarse-mode particles that do not travel far from their sources.

565   The results presented here confirm the dust emission potential in Northern Canada with satellite observations. The regions identified as dust hotspots are candidates for further research into processes involved in driving dust emission at high latitudes, and also provide an observational basis for evaluating and refining numerical models that are used to simulate the dust cycle and the Earth System impacts of dust.

Appendix
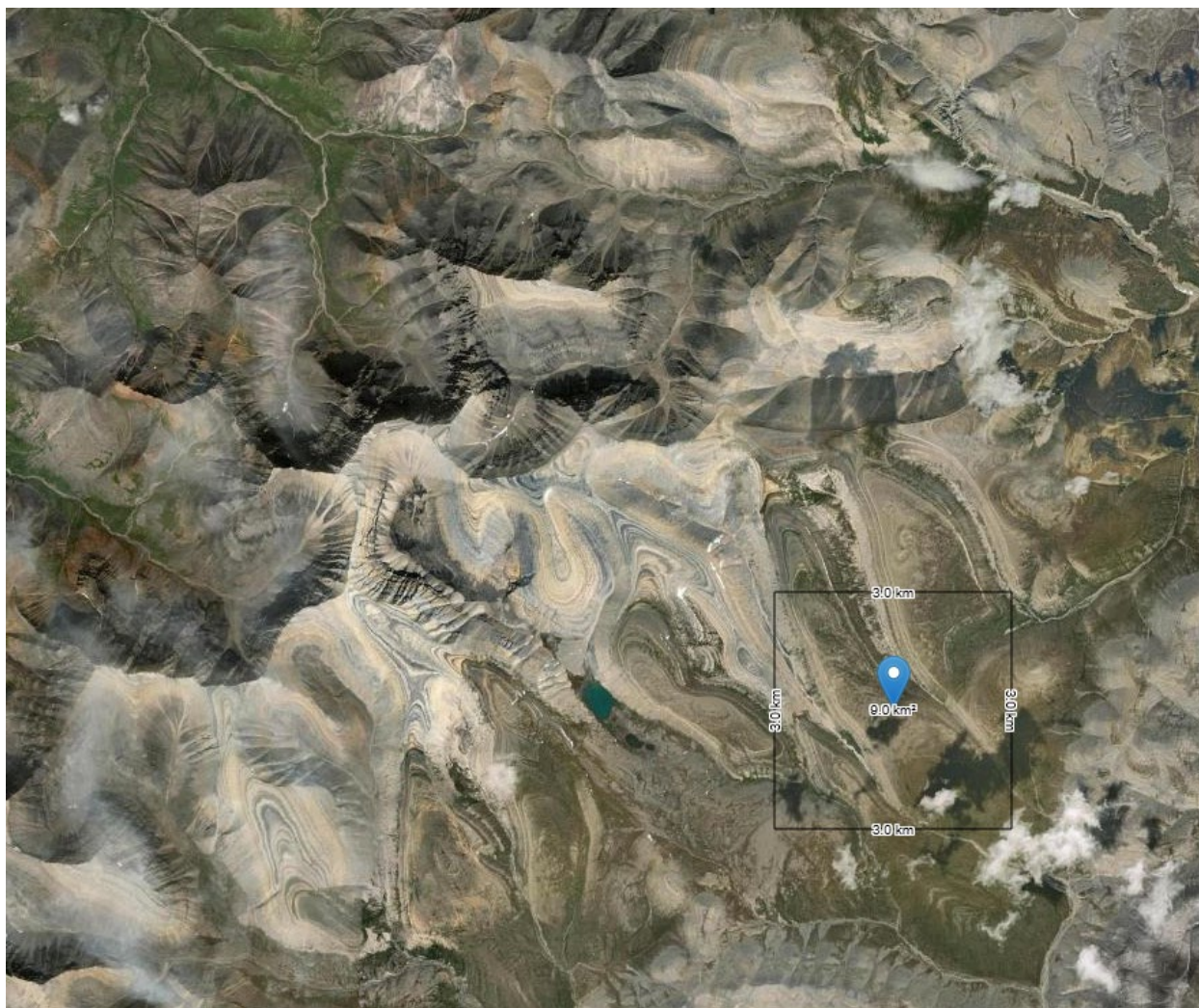
Figure A1. Visible imagery of the potential dust source area in the MacKenzie Mountains (marked by a pink square in Fig. 11). Centre of 9.0 km² box is at 63°N, 126°W with a mean wind speed of 8.13 m/s (predominantly westerly). Topography varies from 900 m to 2300 m in full region shown. Obtained from the Global Wind Atlas version 3.3, a free, web-based application developed, owned and operated by the Technical University of Denmark (DTU). The Global Wind Atlas version 3.3 is released in partnership with the World Bank Group, utilizing data provided by Vortex, using funding provided by the Energy Sector Management Assistance Program (ESMAP). For additional information: https://globalwindatlas.info.
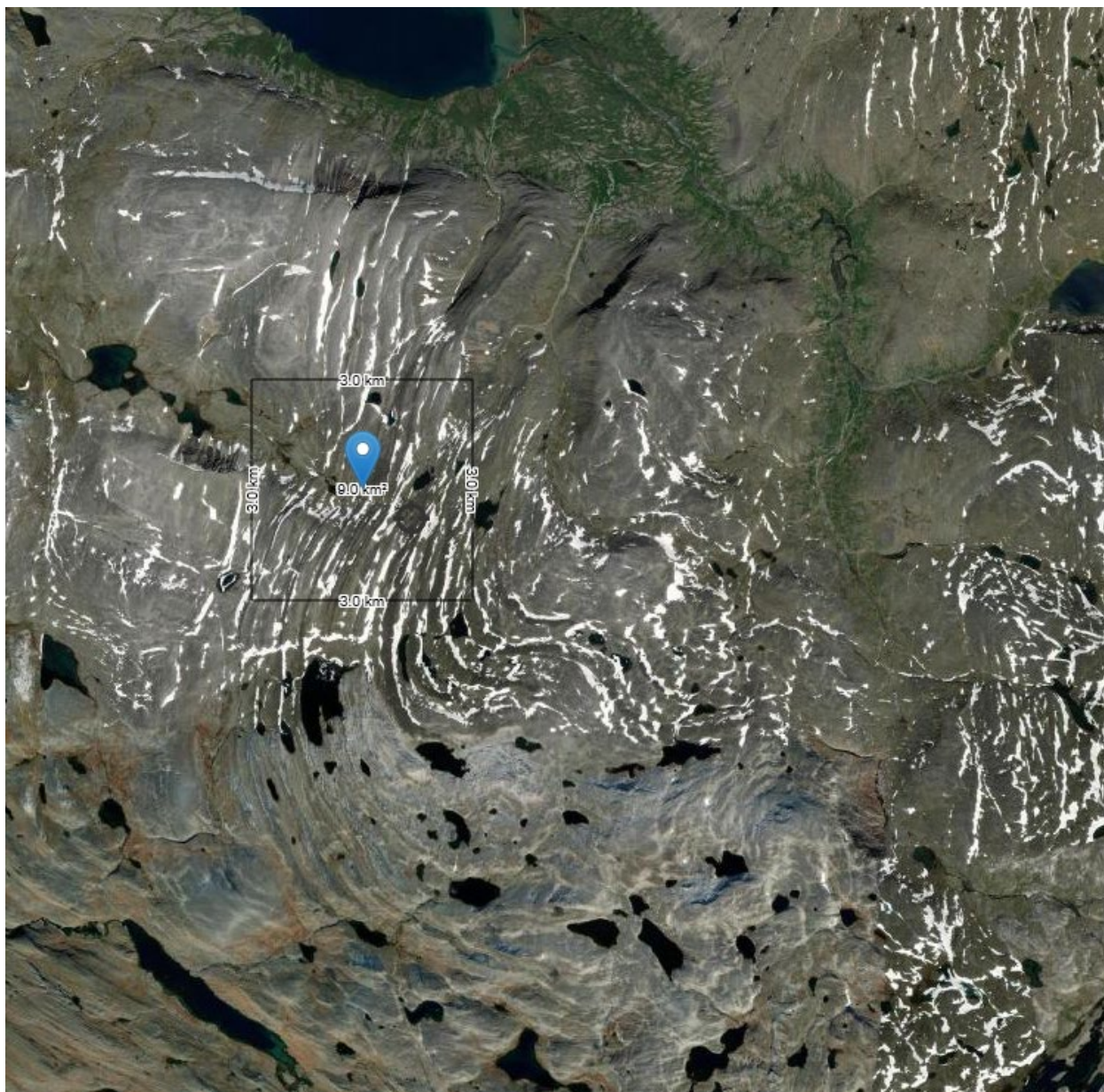
580

Figure A2. Visible imagery of the potential dust source area at the Québec and Labrador border (marked by a blue square in Fig. 11). Centre of 9.0 km² box is at 58.4°N, 65.1°W with a mean wind speed of 11.4 m/s (predominantly westerly). Topography varies from 200 m to 900 m in full region shown. Obtained from the Global Wind Atlas version 3.3, a free, web-based application developed, owned and operated by the Technical University of Denmark (DTU). The Global Wind Atlas version 3.3 is released in partnership with the World Bank Group, utilizing data provided by Vortex, using funding provided by the Energy Sector Management Assistance Program (ESMAP). For additional information: https://globalwindatlas.info.

Data availability. The high-resolution MODIS AOD and DOD data products underlying this study are available upon request.

590   *Author contributions.* AW and IA both conceived of and designed the study. IA performed data processing and analysis. Both authors examined and interpreted the results. IA prepared the manuscript while AW edited it.

Competing interests. The authors declare that they have no conflict of interest.

595   *Acknowledgements.* The authors thank Dr. Deanne Van Rooyen and Dr. Jacob Hanley for helpful discussions about the geological features and dust-emission potential of the MacKenzie Mountains and Québec / Labrador. Any errors of discussion presented here are our own.

Financial support. This research has been supported by the Canadian Space Agency (grant no. 21SUASMDAC), the Canadian
600   National Sciences and Engineering Research Council through the Discovery Grants Programme (grant no. RGPIN-2014-03888, RGPIN-2022-05225), and Saint Mary's University.

References

AboEl-Fetouh, Y., O'Neill, N. T., Ranjbar, K., Hesaraki, S., Abboud, I., and Sobolewski, P. S.: Climatological-scale analysis of intensive and semi-intensive aerosol parameters derived from AERONET retrievals over the Arctic, *Journal of Geophysical*
605   *Research: Atmospheres, 125*, e2019JD031569, https://doi.org/10.1029/2019JD031569, 2020.

Anderson, T. L., Wu, Y. H., Chu, D. A., Schmid, B., Redemann, J., and Dubovik, O.: Testing the MODIS satellite retrieval of aerosol fine-mode fraction, J. *Geophys. Res.-Atmos., 110*, D18204, https://doi.org/10.1029/2005jd005978, 2005.

610   Baddock, M. C., Ginoux, P., Bullard, J. E., and Gill, T. E.: Do MODIS-defined dust sources have a geomorphological signature?, *Geophys. Res. Lett., 43,* 2606–2613, https://doi:10.1002/2015GL067327, 2016.

Boydell, A. N. and Rutter, N. W.: Surficial Geology and Geomorphology, Root River, District of Mackenzie, *Geological Survey of Canada, Preliminary Map*, 12-1979, 1980.
615

Brouard, E., Roy, M., Dubé-Loubert, H., Lamarche, O., and Hébert, S.: Carte des dépôts de surface de la province de Québec: rapport sur les méthodes et les données: MB 2020-10, 1:2 500 000, *Ministère de l'Énergie et Ressources naturelles, Québec*, 2020.

620   Bullard, J. E.:   Contemporary glacigenic inputs to the dust cycle, *Earth Surf. Proc. Land, 38*,71–89,
        https://doi:10.1002/esp.3315, 2013.

        Bullard, J. E., Baddock, M., Bradwell, T., Crusius, J., Darlington, E., Gaiero, D., Gasso, S., Gisladottir, G., Hodgkins, R.,
        McCulloch, R.: High-latitude dust in the Earth system, *Reviews of Geophysics, 54*, 447–485, 2016.
625
        Danielson, J.J., and Gesch, D.B.: Global multi-resolution terrain elevation data 2010 (GMTED2010), U.S. Geological Survey
        Open-File Report 2011-1073, 26 p., http://pubs.usgs.gov/of/2011/1073/pdf/of2011-1073.pdf, 2011.

        Dansie, A. P., Thomas, D.S.G., Wiggs, G.F.S., Baddock, M.C, and Ashpole, I.: Plumes and blooms – Locally-sourced Fe-rich
630   aeolian mineral dust drives phytoplankton growth off southwest Africa, *Science of The Total Environment, 829*,
        https://doi.org/10.1016/j.scitotenv.2022.154562, 2022.

        Davis, N. N., Badger, J., Hahmann, A. N., Hansen, B. O., Mortensen, N. G., Kelly, M., Larsén, X. G., Olsen, B. T., Floors, R.
        Lizcano, G., Casso, P., Lacave, O., Bosch, A., Bauwens, I., Knight, O. J., van Loon, A. P., Fox, R., Parvanyan, T., Krohn
635   Hansen, S. B., Heathfield, D., Onninen, M., Drummond, R.: The Global Wind Atlas: A high-resolution dataset of
        climatologies and associated web-based application, *Bulletin of the American Meteorological Society*, 104 (8), E1507-E1525,
        https://doi:10.1175/BAMS-D-21-0075.1, 2023.

        Dubovik, O., Holben, B., Eck, T. F., Smirnov, A., Kaufman, Y. J., King, M. D., Tanré, D. and Slutsker, I.: Variability of
640   absorption and optical properties of key aerosol types observed in worldwide locations, *J. Atmos. Sci., 59*,590–608, 2002.

        Duk-Rodkin, A. and Huntley, D. H.: Surficial geology, Dahadinni River, Northwest Territories, NTS 95-N southwest.
        prelim., *Geological Survey of Canada, Canadian Geoscience Map*, 297, 2018.

645   Eck, T. F., Holben, B. N., Reid, J. S., Dubovik, O., Smirnov, A., O'Neill, N. T., Slutsker, I., and Kinne, S.: Wavelength
        dependence of the optical depth of biomass burning, urban, and desert dust aerosols, *J. Geophys. Res., 104*(D24), 31,333–
        31,349, 1999.

        Giles, D. M., Sinyuk, A., Sorokin, M. G., Schafer, J. S., Smirnov, A., Slutsker, I., Eck, T. F., Holben, B. N., Lewis, J. R.,
650   Campbell, J. R., Welton, E. J., Korkin, S. V., and Lyapustin, A. I.: Advancements in the Aerosol Robotic Network
        (AERONET) Version 3 database – automated near-real-time quality control algorithm with improved cloud screening for Sun
        photometer aerosol optical depth (AOD) measurements, *Atmos. Meas. Tech., 12,* 169–209, https://doi.org/10.5194/amt-12-
        169-2019, 2019.

655   Ginoux, P., Prospero, J. M., Gill, T. E., Hsu, N. C., and Zhao, M.: Global-scale attribution of anthropogenic and natural dust sources and their emission rates based on MODIS Deep Blue aerosol products, *Rev. Geophys., 50*, RG3005, https://doi:10.1029/2012RG000388, 2012.

Groot Zwaaftink, C. D., Grythe, H., Skov, H., and Stohl, A.: Substantial contribution of northern high-latitude sources to
660   mineral dust in the Arctic, *Journal of Geophysical Research: Atmospheres, 121*(22), 13,678–13,697. https://doi:10.1002/2016JD025482, 2016.

Gulev, S.K., Thorne, P.W., Ahn, J. , Dentener, F.J., Domingues, C.M., Gerland, S., Gong, D., Kaufman, D.S., Nnamchi, H.C., Quaas, J., Rivera, J.A., Sathyendranath, S., Smith, S.L., Trewin, B., von Schuckmann, K., and Vose, R. S.: Changing State of
665   the Climate System. In *Climate Change 2021: The Physical Science Basis. Contribution of Working Group I to the Sixth Assessment Report of the Intergovernmental Panel on Climate Change* [Masson-Delmotte, V., P. Zhai, A. Pirani, S.L. Connors, C. Péan, S. Berger, N. Caud, Y. Chen, L. Goldfarb, M.I. Gomis, M. Huang, K. Leitzell, E. Lonnoy, J.B.R. Matthews, T.K. Maycock, T. Waterfield, O. Yelekçi, R. Yu, and B. Zhou (eds.)]. Cambridge University Press, Cambridge, United Kingdom and New York, NY, USA, pp. 287–422, 2021.

670
Hersbach H., Bell B., Berrisford P., et al.: The ERA5 global reanalysis, *Q. J. R. Meteorol. Soc, 146*, 1999-2049, https://doi.org/10.1002/qj.3803, 2020.

Holben, B. N., Eck, T. F., Slutsker, I., Tanré, D., Buis, J. P., Setzer, A., Vermote, E., Reagan, J. A., Kaufman, Y. J., Nakajima,
675   T., Lavenu, F., Jankowiak, I., and Smirnov, A.: AERONET – A federated instrument network and data archive for aerosol characterization, *Remote Sens. Environ., 66*, 1–16, https://doi.org/10.1016/S0034-4257(98)00031-5, 1998.

Hsu, N. C., Jeon, M.-J., Bettenhausen, C. , Sayer, A. M., Hansell, R., Seftor, C. S., Huang, J., and Tsay, S.-C.: Enhanced Deep Blue aerosol retrieval algorithm: The second generation, *J. Geophys. Res. Atmos., 118*, 9296–9315,
680   https://doi:10.1002/jgrd.50712, 2013.

Hsu, N. C., Lee, J., Sayer, A. M., Kim, W., Bettenhausen, C., and Tsay, S.-C.: VIIRS Deep Blue aerosol products over land: Extending the EOS long-term aerosol data records, *Journal of Geophysical Research: Atmospheres, 124*, 4026–4053, https://doi.org/10.1029/2018JD029688, 2019.

685

Huck, R., Bryant, R.G., and King, J.: The (mis)identification of high-latitude dust events using remote sensing methods in Yukon, Canada: a sub-daily variability analysis, *Atmos. Chem. Phys., (23)*, 6299-6318, https://doi.org/10.5194/acp-23-6299-2023, 2023.

690 Kim, M.-H., Omar, A. H., Tackett, J. L., Vaughan, M. A., Winker, D. M., Trepte, C. R., Hu, Y., Liu, Z., Poole, L. R., Pitts, M. C., Kar, J., and Magill, B. E.: The CALIPSO version 4 automated aerosol classification and lidar ratio selection algorithm, *Atmos. Meas. Tech., 11*, 6107–6135, https://doi.org/10.5194/amt-11-6107-2018, 2018.

Kok, J. F., Ward, D. S., Mahowald, N. M., & Evan, A. T.: Global and regional importance of the direct dust-climate feedback, 695 *Nature Communications, 9*(1), https://doi.org/10.1038/s41467-017-02620-y, 2018.

Kok, J. F., Ridley, D. A., Zhou, Q., Miller, R. L., Zhao, C., Heald, C. L., Ward, D. S., Albani, S., and Haustein, K.: Smaller desert dust cooling effect estimated from analysis of dust size and abundance, *Nat. Geosci., 10*, https://doi.org/10.1038/Ngeo2912, 2017.

700

Kok, J. F.: A scaling theory for the size distribution of emitted dust aerosols suggests climate models underestimate the size of the global dust cycle, *Proceedings of the National Academy of Sciences*, 108(3), 1016-1021, https://doi.org/10.1073/pnas.1014798108, 2011.

705 Kylling A., Groot Zwaaftink, C. D., & Stohl, A.: Mineral dust instantaneous radiative forcing in the Arctic, *Geophysical Research Letters, 45*, 4290–4298, https://doi.org/10.1029/2018GL077346, 2018.

Meinander, O., Dagsson-Waldhauserova, P., Amosov, P., Aseyeva, E., Atkins, C., Baklanov, A., et al.: Newly identified climatically and environmentally significant high-latitude dust sources, *Atmos. Chem. Phys., 22*, 11889–11930, 710 https://doi:10.5194/acp-22-11889-2022, 2022.

Nogueira, J., Evangelista, H., Valeriano, C.d.M. et al.: Dust arriving in the Amazon basin over the past 7,500 years came from diverse sources, *Commun Earth Environ 2*, 5, https://doi.org/10.1038/s43247-020-00071-w, 2021.

715 Occhietti, S., Govare, É., Klassen, R., Parent, M. and Vincent, J.S.: Late Wisconsinan-Early holocene deglaciation of Québec-Labrador, in *Developments in Quaternary Sciences* (Vol. 2, pp. 243-273), 2004.

Omar, A. H., Winker, D. M., Vaughan, M. A., Hu, Y., Trepte, C. R., Ferrare, R. A., Lee, K. P., Hostetler, C. A., Kittaka, C., Rogers, R. R., and Kuehn, R. E.: The CALIPSO Automated Aerosol Classification and Lidar Ratio Selection Algorithm, *J. Atmos. Ocean. Tech., 26,* 1994–2014, https://doi.org/10.1175/2009JTECHA1231.1, 2009.

Platnick, S., King, M., Wind, B., and Ridgway, W.: MODIS Atmosphere L2 Joint Atmosphere Product. NASA MODIS Adaptive Processing System, Goddard Space Flight Center, doi:10.5067/MODIS/MODATML2.061; https://doi:10.5067/MODIS/MYDATML2.061, 2017.

Prijith, S.S., Aloysius, M., and Mohan, M.: Global aerosol source/sink map, *Atmospheric Environment, 80*, 533-539, https://doi.org/10.1016/j.atmosenv.2013.08.038, 2013.

Prospero, J.M., Ginoux, P., Torres, O., Nicholson, S.E., Gill, T. E.: Environmental characterization of global sources of atmospheric soil dust identified with the NIMBUS 7 Total Ozone Mapping Spectrometer (TOMS) absorbing aerosol product, *Reviews of Geophysics, 40(1)*, 1002, https://doi.org/10.1029/2000RG000095, 2002.

Prospero, J. M.: Long-range transport of mineral dust in the global atmosphere: Impact of African dust on the environment of the southeastern United States, *Proceedings of the National Academy of Sciences*, 96(7), 3396-3403, https://doi.org/10.1073/pnas.96.7.3396, 1999.

Pu, B. and Ginoux, P.: The impact of the Pacific Decadal Oscillation on springtime dust activity in Syria, *Atmos. Chem. Phys., 16*, 13431–13448, https://doi.org/10.5194/acp-16-13431-2016, 2016.

Pu, B., Ginoux, P., Guo, H., Hsu, C. N., Kimball, J., Marticorena, B., Malyshev, S., Naik, V., O'Neill, N. T., García-Pando, C. P., Paireau, J., Prospero, J. M., Shevliakova, E., and Zhao, M.: Retrieving the global distribution of the threshold of wind erosion from satellite data and implementing it into the Geophysical Fluid Dynamics Laboratory land-atmosphere model (GFDL AM4.0/LM4.0), *Atmos. Chem. Phys., 20*(1), 55–81, https://doi.org/10.5194/acp-20-55-2020, 2020.

Ranjbar, K., O'Neill, N. T., Ivanescu, L., King, J., and Hayes, P. L.: Remote sensing of a high- Arctic, local dust event over Lake Hazen (Ellesmere Island, Nunavut, Canada), *Atmos. Environ., 246*, 118102, https://doi.org/10.1016/j.atmosenv.2020.118102, 2021.

Sarangi, C., Qian, Y., Rittger, K., Leung, L. R., Chand, D., Bormann, K. J., & Painter, T. H.: Dust dominates high-altitude snow darkening and melt over high-mountain Asia, *Nature Climate Change*, https://doi.org/10.1038/s41558-020-00909-3, 2020.

Sayer, A. M., Hsu, N. C., Bettenhausen, C., Jeong, M.-J., and Meister, G.: Effect of MODIS Terra radiometric calibration improvements on Collection 6 Deep Blue aerosol products: Validation and Terra/Aqua consistency, *J. Geophys. Res. Atmos.,* 755 *120,* 12, 157–12, 174, https://doi:10.1002/2015JD023878, 2015.

Tegen, I.: Modeling the mineral dust aerosol cycle in the climate system, Quat. Sci. Rev., 22, 1821-1834, 2003.

Tackett, J. L., Winker, D. M., Getzewich, B. J., Vaughan, M. A., Young, S. A., and Kar, J.: CALIPSO lidar level 3 aerosol 760 profile product: version 3 algorithm design, *Atmos. Meas. Tech., 11*, 4129–4152, https://doi.org/10.5194/amt-11-4129-2018. 2018.

Tobo, Y., Adachi, K., DeMott, P. J., Hill, T. C. J., Hamilton, D. S., Mahowald, N. M., … Koike, M.: Glacially sourced dust as a potentially significant source of ice nucleating particles, *Nature Geoscience, 12(4)*, 253–258. 765 https://doi.org/10.1038/s41561-019-0314-x, 2019.

Todd, M. C., and Cavazos-Guerra, C.: Dust aerosol emission over the Sahara during summertime from Cloud-Aerosol Lidar with Orthogonal Polarization (CALIOP) observations, *Atmospheric Environment, 128*, 147-157, https://doi.org/10.1016/j.atmosenv.2015.12.037, 2016.

770

Tomasi, C., Kokhanovsky, A. A., Lupi, A., Ritter, C., Smirnov, A., O'Neill, N. T., et al.: Aerosol remote sensing in polar regions, *Earth-Science Reviews, 140*, 108–157. https://doi.org/10.1016/j.earscirev.2014.11.001, 2015.

Vukovic, A.: Global high-resolution dust source map, InDust webinar, https://cost-indust.eu/sites/default/files/2021-775 04/vukovic_indust_webinar_april2021.pdf (last access: 11 January 2024), 21 April 2021.

Vukovic, A.: Sand and dust storm source mapping, in United Nations Convention to Combat Desertification (UNCCD), (2022), *Sand and Dust Storms Compendium: Information and Guidance on Assessing and Addressing the Risks*, Bonn, Germany, 2022.

780

Washington, R. M., Todd, M., Middleton, N. J., and Goudie, A. S.: Dust-storm areas determined by the Total Ozone Monitoring Spectrometer and surface observations, *Ann. Assoc. Am. Geogr., 93*, 297–313, https://doi:10.1111/1467-8306.9302003, 2003.

785   Winker, D. M., Pelon, J., Coakley Jr, J. A., Ackerman, S. A., Charlson, R. J., Colarco, P. R., Flamant, P., Fu, Q., Hoff, R. M., Kittaka, C., Kubar, T. L., Le Treut, H., McCormick, M. P., Mégie, G., Poole, L., Powell, K., Trepte, C., Vaughan, M. A., and Wielicki, B. A.: The CALIPSO mission: A global 3D view of aerosols and clouds, *Bull. Amer. Meteor. Soc., 91*, 1211–1229, https://doi.org/10.1175/2010BAMS3009.1, 2010.

790   Wiacek, A., Peter, T. and Lohmann, U.: The potential influence of Asian and African mineral dust on ice, mixed-phase and liquid water clouds, *Atm. Chem. Phys., 10*, 8649–8667, https://doi:10.5194/acp-10-8649-2010, 2010.

Yang, A., Tan, Q., Rajapakshe, C., and Chin, M.: Global premature mortality by dust and pollution PM2.5 estimated from aerosol reanalysis of the modern-era retrospective analysis for research and applications, version 2, *Front. Environ. Sci., 10*, 795   https://doi.org/10.3389/fenvs.2022.975755, 2022.

Zhao, X., Huang, K., Fu, J. S., and Abdullaev, S. F.: Long-range transport of Asian dust to the Arctic: identification of transport pathways, evolution of aerosol optical properties, and impact assessment on surface albedo changes, *Atmos. Chem. Phys.*, 22, 10389–10407, https://doi.org/10.5194/acp-22-10389-2022, 2022.